Article:

Wang, Z. orcid.org/0000-0001-8142-1154, Yun, X. orcid.org/0000-0002-5179-4731, Wang, Y. et al. (2 more authors) (2023) Numerical study and design of swage-locking pinned aluminium alloy shear connections. Thin-Walled Structures, 190. 110949. ISSN 0263-8231

https://doi.org/10.1016/j.tws.2023.110949

Wang ZX, Yun X, Wang YQ, Ma CY, Yan JB. Numerical study and design of swage-locking pinned aluminium alloy shear connections. Thin-Walled Structures, 2023(0263-8231)

Numerical study and design of swage-locking pinned aluminium alloy shear connections

Zhongxing Wang[1,2,3], Xiang Yun[4], Yuanqing Wang[5], Chunyin Ma[2] and Jia-Bao Yan[2]

[1]*Key Laboratory of Earthquake Engineering Simulation and Seismic Resilience of China Earthquake Administration (Tianjin University), Tianjin 300350, PR China*

[2]*School of Civil Engineering, Tianjin University, Tianjin 300350, PR China*

[3]*Key Laboratory of Seismic Engineering Technology, Sichuan Province, Southwest Jiaotong University, Chengdu 610031, PR China*

[4]*Department of Civil and Structural Engineering, University of Sheffield, Sheffield S1 3JD, UK*

[5]*Department of Civil Engineering, Tsinghua University, Beijing 10084, PR China*

Abstract

Swage-locking pinned connections are becoming increasingly popular in aluminium alloy structures. This paper presents a comprehensive numerical study into the structural performance and design of swage-locking pinned aluminium alloy shear connections. Finite element (FE) models, taking account of the influence of stress triaxiality on the fractural behaviour of swage-locking pinned aluminium alloy shear connections, were first established and validated against existing test data from the authors. Complementary measurements on the preload of fasteners and the friction coefficient between aluminium plates were also performed for FE model input and verification. Upon validation of the developed FE models for swage-locking pinned aluminium alloy shear connections, parametric studies were carried out, aiming at

expanding the structural performance data over a wider range of aluminium alloy grades and geometric configurations, including end distances, inner-plate thicknesses, pin diameters and edge distances. Based on the obtained results, the influence of the friction coefficient between aluminium plates, as well the key material and geometrical parameters, on the resistances of aluminium alloy connections was discussed. Finally, revised design methods for determining the ultimate resistances of swage-locking pinned aluminium alloy shear connections were proposed. It was shown that the design proposals in the present study provide more accurate and less scattered resistance predictions than existing codified design approaches for aluminium alloy shear connections.

Keywords

Aluminium alloy; Design method; Friction coefficient; Numerical study; Shear connections; Swage-locking pin

1. Introduction

Recent decades have witnessed an increasing use of aluminium alloys in structural applications [1], owing to their superior corrosion resistance, high strength-to-weight ratio, ease of extrusion and fabrication and excellent recyclability [2]. In spite of these favourable features, the poor weldability of the structural aluminium alloys poses a challenge to effectively join aluminium elements. Fastener connections are therefore extensively used in aluminium alloy structures to avoid strength reduction resulted from the welding. The structural behaviour of aluminium alloy fastener connections has been investigated in a number of studies. As early as 1937, Miller [3] conducted a series of tests on both bolted and riveted aluminium alloy shear connections, finding that the bearing resistances of these connection were influenced by mainly four parameters: material strength, fastener diameter, plate thickness and edge distance. Menzemer et al. [4-6] performed thorough experimental and numerical studies on the bearing and block shear behaviour of aluminium alloy bolted connections, the results of which were utilised to assess the accuracy of the design rules specified in the Aluminum Design Manual (ADM) [7]. Wang et al. [8] conducted experiments on a total of 20 aluminium alloy bolted connections and proposed a new design method for accurately predicting the bolt shear force in long connections. Kim and co-workers [9-11] conducted systematic investigations on 6061-T6 and 7075-T6 aluminium alloy single shear connections and proposed new design equations for connections that are susceptible to out-of-plane deformations (i.e. curling).

As indicated in the above literature review, the majority of research to date has been focused on the structural performance of aluminium alloy bolted connections. With the ongoing advances in fastener manufacturing, novel fasteners (e.g. Hollo bolt [12], Molabolt [13] and swage-locking pin) that feature more favourable mechanical properties are becoming increasingly popular in structural engineering. The swage-locking pin is a new category of fasteners, which exhibits good resistance to vibration and loosening and can be rapidly installed by using a hydraulic rivet gun [14]. In addition, the use of swage-locking pins can avoid the thread galling failure which is commonly seen in conventional stainless steel bolts [15]. These above advantages greatly increased the application of swage-locking pins in aluminium alloy structures, typical examples of which are the Rafel Gallery in Shanghai [16] and the Usnisa Palace in Nanjing [17]. The experimental investigation in the companion paper [16] revealed that the existing codified methods [18-20] fail to explicitly consider the influence of material characteristics and friction on the resistances of swage-locking pinned aluminium alloy shear connections, resulting in somewhat inaccurate resistance predictions. The structural performance and design of swage-locking pinned aluminium alloy shear connections, which has not been systematically studied to date, is therefore the focus of the present study.

A comprehensive numerical study into the structural behaviour of swage-locking pinned aluminium alloy shear connections is presented herein. Prior to the establishment of finite element (FE) models, complementary measurements on the preload of swage-locking pins and the friction coefficient between aluminium alloy plates were carried out for FE model input and verification. FE models, taking account of the influence of stress triaxiality on the fractural behaviour of swage-locking pinned aluminium alloy shear connections, were then developed and validated against the test results reported in the companion paper [16]. The validated models were subsequently employed to perform parametric studies considering a wider coverage of key parameters that affect the behaviour and resistance of swage-locking pinned aluminium alloy shear connections; these include the aluminium alloy grade, the friction coefficient between aluminium alloy plates and the geometric configurations of shear connections (e.g. end distance, inner-plate thickness, pin diameter and edge distance). Finally, based on the obtained results, revised design equations for determining the ultimate resistance of swage-locking pinned aluminium alloy shear connections failing in different failure modes are proposed.

2. Review of previous experimental studies and complementary measurements

In this section, a summary of previous experimental studies on swage-locking pinned aluminium alloy shear connections carried out by Wang et al. [16] is presented. In addition, complementary measurements of the preload of fasteners and the friction coefficient between aluminium alloy plates were performed, providing essential input parameters for model input and validation, and are also presented in this section.

2.1. Shear connection tests [16]

A total of 23 swage-locking pinned aluminium alloy shear connections of four different aluminium alloy grades (i.e. 6061-T6, 6063-T5, 6082-T6 and 7A04-T6) and three different configurations, as shown in Fig. 1, were tested. Prior to the shear connection tests, the material properties of the four investigated aluminium alloys were determined by tensile symmetric tests, as summarised in Table 1 [16]. Four different failure modes, including shear-out, bearing, block shear and net section tension fracture (typical examples of which are illustrated in Fig. 2) were observed and analysed in [16]. The test ultimate resistances (P_{Test}) and failure modes of the tested specimens are summarised in Table 2, along with the material and geometric properties, where e_1 is the end distance, e_2 is the edge distance, and p_1 and p_2 are the pitch and gauge distances, respectively, as shown in Fig. 1. More details regarding the test setup and specimen configurations can be found in [16].

Table 1. Measured material properties of different aluminium alloy inner plates of the shear connection test specimens [16]

Material	E (MPa)	$f_{0.2}$ (MPa)	f_u (MPa)	n	$f_u/f_{0.2}$	ε_u (%)
6061-T6	68100	275	320	23.4	1.17	8.7
6063-T5	68300	170	225	12.8	1.33	8.2
6082-T6	69200	335	375	36.8	1.11	10.2
7A04-T6	70900	545	595	42.3	1.09	8.4

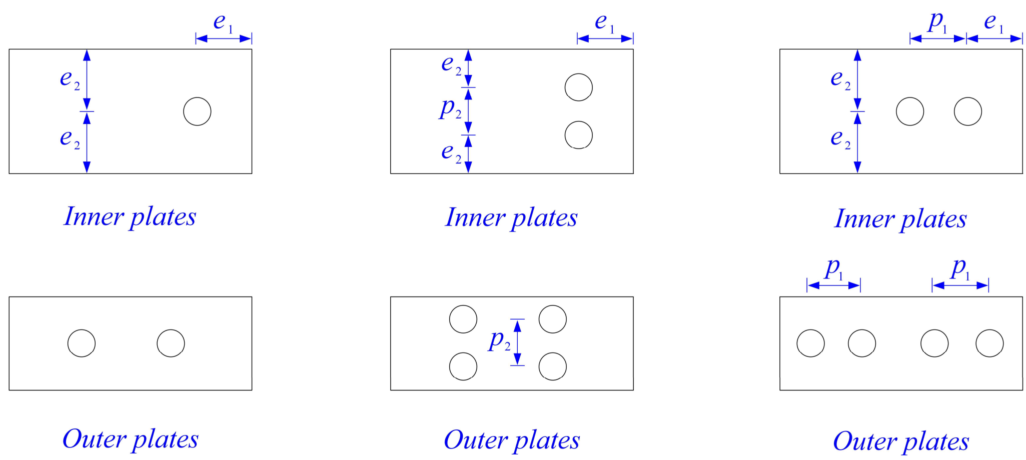

Type1: Connection with single swage-locking pin (CS) **Type2**: Connection with double swage-locking pins transversely (CDT) **Type3**: Connection with double swage-locking pins longitudinally (CDL)

Fig. 1. Configurations of tested specimens [16]

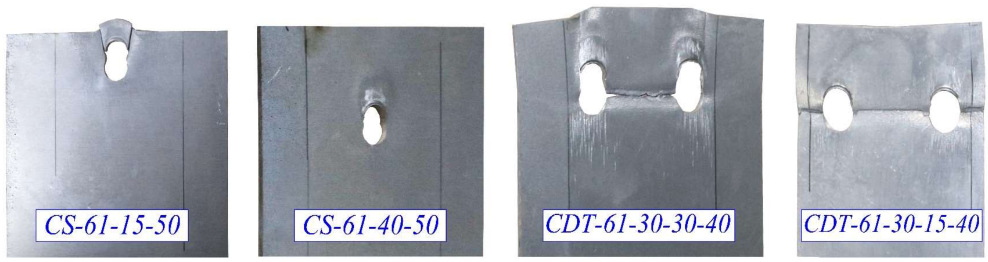

(a) Shear-out (b) Bearing (c) Block-shear (d) Net section

Fig. 2. Typical failure modes of tested specimens [16]

Table 2. Summary of material and geometric properties and experimental results of tested specimens [16]

Type of connection	Specimen label	Alloy	e_1 (mm)	e_2 (mm)	p_1 (mm)	p_2 (mm)	P_{Test} (kN)	Failure modes
Type 1	CS-61-10-50	6061-T6	10	50	–	–	20.6	SO[a]
Type 1	CS-61-15-50	6061-T6	15	50	–	–	25.3	SO[a]
Type 1	CS-61-20-50	6061-T6	20	50	–	–	31.2	SO[a]
Type 1	CS-61-30-50	6061-T6	30	50	–	–	41.6	SO[a]
Type 1	CS-61-40-50	6061-T6	40	50	–	–	50.2	B[b]
Type 1	CS-63-15-50	6063-T5	15	50	–	–	19.6	SO[a]
Type 1	CS-63-40-50	6063-T5	40	50	–	–	38.6	B[b]
Type 1	CS-82-15-50	6082-T6	15	50	–	–	26.8	SO[a]
Type 1	CS-82-40-50	6082-T6	40	50	–	–	52.5	B[b]
Type 1	CS-04-15-50	7A04-T6	15	50	–	–	34.5	SO[a]
Type 1	CS-04-40-50	7A04-T6	40	50	–	–	66.7	B[b]
Type 2	CDT-61-30-10-40	6061-T6	30	10	–	40	54.1	NS[c]
Type 2	CDT-61-30-15-40	6061-T6	30	15	–	40	67.5	NS[c]
Type 2	CDT-61-30-20-40	6061-T6	30	20	–	40	80.4	NS[c]
Type 2	CDT-61-30-30-40	6061-T6	30	30	–	40	81.8	BS[d]
Type 2	CDT-61-30-40-20	6061-T6	30	40	–	20	60.7	BS[d]
Type 2	CDT-61-30-40-25	6061-T6	30	40	–	25	64.4	BS[d]
Type 2	CDT-61-30-40-30	6061-T6	30	40	–	30	73.2	BS[d]
Type 2	CDT-61-30-40-40	6061-T6	30	40	–	40	85.7	BS[d]
Type 3	CDL-61-30-50-20	6061-T6	30	50	20	–	63.4	SO[e]/SO[f]
Type 3	CDL-61-30-50-25	6061-T6	30	50	25	–	67.5	SO[e]/SO[f]
Type 3	CDL-61-30-50-30	6061-T6	30	50	30	–	75.5	SO[e]/SO[f]
Type 3	CDL-61-30-50-40	6061-T6	30	50	40	–	84.5	SO[e]/B[f]

Note: [a]SO: shear-out; [b]B: bearing failure; [c]NS: net section failure; [d]BS: block shear.
[e]Failure mode of downstream pin hole; [f]failure mode of upstream pin hole.

2.2. Complementary measurements of preload and friction coefficient

As a complement to the tests on the swage-locking pinned aluminium alloy shear connections, the preload of swage-locking pins and the friction coefficient between aluminium alloy plates were carefully measured to provide essential input parameters for numerical modelling and validation.

Two aluminium alloy plates were connected together by a swage-locking pin, in which a preload was applied by using a hydraulic rivet gun [16]. The preload in the swage-locking pin was measured using a specially devised load cell with a maximum capacity of 30 kN, as shown in Fig. 3. During the fastening process, readings from the load cell fluctuated significantly at the beginning then became constant at the end; the stable value was taken as the measured preload of the swage-locking pin. Six repeated measurements were carried out to assess the variability of the results. The measured preloads were 22.3, 24.5, 24.4, 23.8, 23.5 and 23.8 kN, showing a high level of consistency. The mean value of 23.7 kN was taken as the applied preload ($F_{p,C}$) of swage-locking pins and employed in the numerical simulations described in Section 3.

The preload loss of fasteners can have a significant influence on the behaviour of aluminium alloy connections. To quantitatively characterise the preload loss in swage-locking pins, the time histories of preload relaxation of three swage-locking pins were monitored over a period of 12 hours using the same measuring instrument as shown in Fig. 3. Note that it has been found that most of the preload relaxation of fasteners takes place within 12 hours after tightening [21-23]. The time histories of the relative residual preload (i.e. the ratio of the residual preload $F_{p,r}$ at time after tightening T in hours to the initial preload $F_{p,C}$) of the three investigated swage-locking pins are shown in Fig. 4. It can be observed that the majority of preload relaxation took place within the first 6 hours of tightening, and the preload loss at the 12-hour period is within 2% of the initial preload $F_{p,C}$, which is substantially less than that of the conventional stainless steel and carbon steel bolts [21-23].

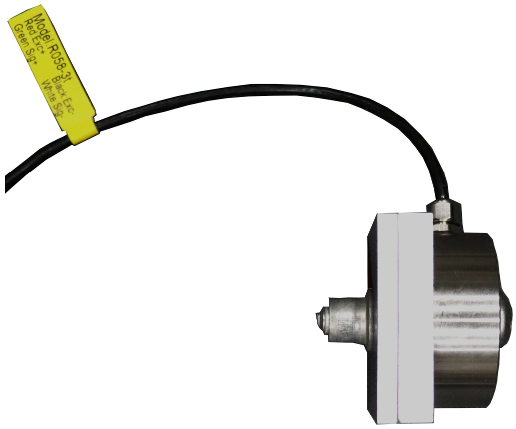

Fig. 3. Specially devised load cell for measurement of preload in swage-locking pins

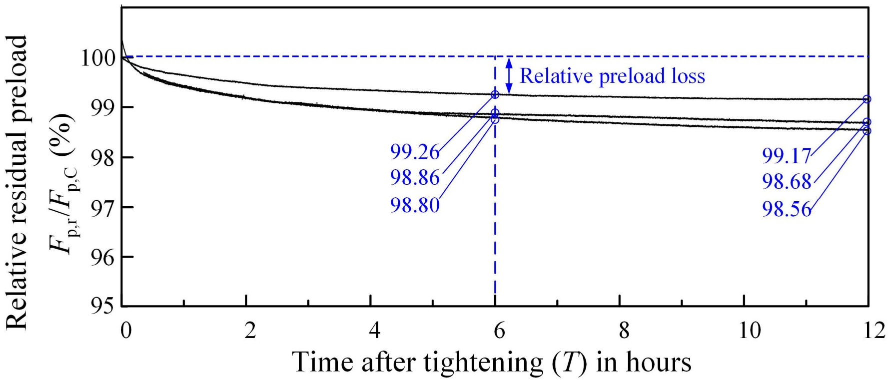

Fig. 4. Time histories of relative residual preload over a period of 12 hour after tightening for the measured three swage-locking pins

Measurements on the friction coefficient between aluminium alloy plates were also conducted in accordance with JGJ 82–2011 [24] and EN 1090-2: 2018 [25] as part of the present study. The specimen used for the slip tests comprised two aluminium alloy inner plates and two aluminium alloy outer plates, which were connected using four swage-locking pins arranged in the loading direction, as shown in Fig. 5, in which d_{pin} is the nominal diameter of the pin, and S1, S2, S3 and S4 represent different slip planes between aluminium alloy plates. Prior to the fastening of the swage-locking pins, the inner plates were pushed inward to permit a maximum slip of 0.84 mm (i.e. the clearance between the hole and the pin shank) to occur before the bearing between the pin shank and the pin hole was initiated. The slip tests were conducted in a 100 kN hydraulic testing machine − the same as that used in the shear connection tests [16]. The tests were conducted under load control at a constant rate of 1 kN/min, satisfying the requirement (i.e. duration of test approximately 10 min to 15 min) specified in EN 1090-2: 2018 [25]. The relative displacements between the inner and outer plates were measured using a video gauge, via which the displacements at six selected positions, marked onto the side surface of the inner (i.e. Points b_1 and b_2 see Fig. 5) and outer (i.e. Points a_1, a_2, c_1 and c_2 see Fig. 5) plates were carefully captured. Two slip tests were performed for each of the four investigated aluminium alloys, with a repeat specimen tested for each aluminium alloy enabling the variability in response between specimens to be evaluated.

A total of four load-slip curves (i.e. representing the four slip planes S1 and S2 or S3 and S4) can be obtained from each test, while the obtained curves were found to almost coincide with each other. According to EN 1090-2: 2018 [25], the slip load F_{Si} is defined as the load corresponding to a slip of 0.15 mm or the peak load prior to the attainment of a slip of 0.15 mm. The friction coefficient μ can be determined according to Eq. (1), where 4 represents the number of slip planes in the slip tests. Note that the measured average initial preload $F_{\mathrm{p,C}}$ was utilised to determine the friction coefficient μ in Eq. (1) as it gives the most conservative friction coefficient value compared to the use of the residual preload at the time when the slip tests were conducted. The obtained friction coefficients for different aluminium alloy plates are summarised in Table 3. It can be observed that the friction coefficients of aluminium alloys are generally lower than those of carbon steels [26].

$$\mu = \frac{F_S}{4F_{p,C}} \tag{1}$$

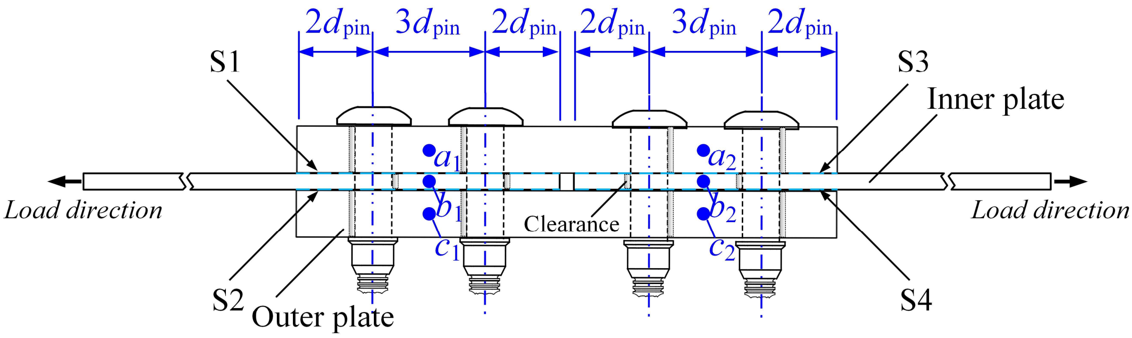

Fig. 5. Geometry of specimens for slip coefficient tests

Table 3. Results of slip coefficient tests

Material	Slip load (kN)					Friction coefficient
	$F_{S12}{}^a$	$F_{S34}{}^a$	$F_{S12}{}^b$	$F_{S34}{}^b$	Mean F_S	
6061-T6	16.45	16.45	17.90	14.84	16.41	0.173
6063-T5	12.82	12.82	-	14.96	13.53	0.143
6082-T6	22.27	21.43	18.22	19.64	20.39	0.215
7A04-T6	-	13.22	12.29	12.29	12.60	0.133

Note: [a] and [b] represent the value was obtained from the first and repeated test group, respectively.

3. Finite element (FE) modelling

Refined three-dimensional finite element (FE) models were developed using the FE package ABAQUS [27] to simulate the behaviour of swage-locking pinned aluminium alloy shear connections under tensile loads. The established FE models were firstly validated against available test results reported in the companion paper [16] and summarised in Section 2, and subsequently adopted for parametric analyses, as descried in Section 4. In this section, the details of the FE modelling assumptions are presented and the key validation results are summarised.

3.1 Modelling assumptions

The eight-noded solid element with reduced integration and hourglass control, referred to as C3D8R in the ABAQUS element library [27], was adopted to model both the aluminium alloy plates and the swage-locking pins. The element has been proved to be suitable for modelling shear connections in a number of previous similar studies [28,29], showing advantages in simulating large deformations and material plasticity and in avoiding the shear-locking problem [30]. As the focus of the present study lies on the failure of the aluminium alloy plates, the threaded region of each swage-locking pin was simply modelled as a stainless steel cylinder without the consideration of the complex interaction between the pin and the collar; the load-carrying capacities of the swage-locking pins under various loading scenarios have been experimentally studied in [31] and the explicit modelling of the load-slip behaviour of swage-locking pins in T-stubs has been described in [32]. A preliminary mesh sensitivity analysis was carried out to determine an appropriate discretisation on the aluminium alloy plates which would be both computational efficiency and sufficiently fine to accurately replicate the structural behaviour of swage-locking pinned shear connections. As shown in Fig. 6, finer meshes were employed to a square region (40 mm × 40 mm) located around the bolt hole where deformation is concentrated due to the contact pressure between the bolt shank and the surface of the bolt hole, while a relatively coarse mesh of approximately 5 mm × 5 mm was used in the remaining region of the aluminium alloy plate. A mesh of three elements was used through the thickness of all the modelled aluminium alloy plates, as illustrated in Fig. 6.

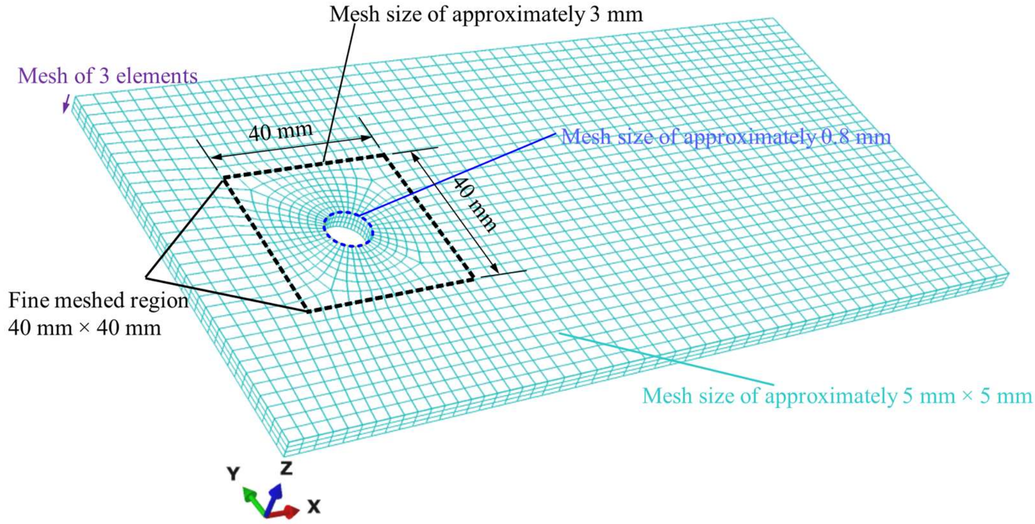

Fig. 6. Selected mesh sizes for aluminium alloy plates

The measured material properties of the four different aluminium alloy grades (i.e. 6061-T6, 6063-T5, 6082-T6 and 7A04-T6 see Table 1) and stainless steel swage-locking pins (see Table 4 in Reference [31]) were adopted in the developed FE models. The single-stage and two-stage Ramberg-Osgood models developed in [33] were utilised to represent the stress-strain relationship of the aluminium alloys and stainless steels, respectively. Note that the measured engineering stress-strain curves were converted into true stress-logarithmic plastic strain curves before inputting into the numerical models, which take into account the change in geometry of shear connections under static loading. The Von Mises yield criterion with the associated Prandtl-Reuss flow rule [34] were employed for all materials in the FE models.

In order to accurately replicate the fracture behaviour of the inner plate under large deformation, the in-built ABAQUS damage model for ductile metals was employed to predict the fracture initiation and evolution. It has been found by Bao and Wierzbicki [35] that apart from the stress intensity, the influence of the stress triaxiality should also be considered for a more accurate prediction of the fracture propagation. The stress triaxiality ($\sigma_H/\bar{\sigma}$) is expressed as the ratio of the hydrostatic stress (σ_H) to the equivalent stress ($\bar{\sigma}$), as given by Eq. (2),

$$\frac{\sigma_H}{\bar{\sigma}} = \frac{(\sigma_1+\sigma_2+\sigma_3)/3}{\sqrt{1/2\left[(\sigma_1-\sigma_2)^2+(\sigma_2-\sigma_3)^2+(\sigma_3-\sigma_1)^2\right]}} \tag{2}$$

where σ_1, σ_2 and σ_3 are principal stresses. The fracture strains (ε_f) of the four investigated aluminium alloys under different range of stress triaxialities have been obtained from material tests carried out by [36-39], as summarised in Table 4; these values were incorporated into the FE models. The ABAQUS features of element deletion was utilised to simulate the fracture within the inner plate of the shear connections.

Table 4. Fracture strains of the four investigated aluminium alloys under different stress triaxialities

6061-T6 [36]		6063-T5 [37]		6082-T6 [38]		7A04-T6 [39]	
$\sigma_H/\bar{\sigma}$	ε_f	$\sigma_H/\bar{\sigma}$	ε_f	$\sigma_H/\bar{\sigma}$	ε_f	$\sigma_H/\bar{\sigma}$	ε_f
-0.5	1.06	0.1	1.79	0.3	1.16	-0.5	0.88
0.0	0.68	0.15	1.62	0.35	0.96	0	0.31
0.1	0.61	0.2	1.47	0.4	0.80	0.1	0.25
0.2	0.55	0.3	1.21	0.45	0.68	0.2	0.21
0.3	0.49	0.4	0.99	0.5	0.58	0.3	0.18
0.4	0.43	0.5	0.81	0.55	0.50	0.4	0.15
0.5	0.38	0.6	0.67	0.6	0.44	0.5	0.13
0.6	0.32	0.7	0.55	0.65	0.39	0.6	0.12
0.7	0.27	0.8	0.45	0.7	0.35	0.7	0.10
0.8	0.23	0.9	0.37	0.75	0.32	0.8	0.09
1.0	0.14	1.0	0.30	0.8	0.30	1.0	0.08

The symmetry of the investigated shear connections with respect to geometries, loading and boundary conditions and failure modes was exploited in the FE models by modelling only half of the shear connection with appropriate boundary conditions employed on the surface of symmetry, as shown in Fig. 7; this modelling assumption helps to decrease the computational time. All degrees of freedom of the loading surface of the inner plate were coupled to a concentric reference point, only alloying translation in X-direction (see Fig. 7), in order to mimic the fixed end boundary condition. The axial load was applied to the reference point by utilising a displacement boundary condition. The swage-locking pins were located eccentrically into the holes in order to eliminate the clearance between the hole and the pin shank [16], enabling direct bearing to be the primary means of load transfer when displacement boundary condition is imposed at the reference point. The preload in the swage-locking pins were simulated using the "Bolt load" option in ABAQUS and the measured average preload as summarised in Section 2.2 were adopted. The ABAQUS "Hard contact" was employed to mimic the interaction at the interfaces between aluminium alloy plates in the normal direction as well as between the surfaces of the plate hole and the pin shank. The interaction at the interfaces between aluminium alloy plates in the tangential direction was simulated by employing a Coulomb friction model, with friction coefficients taken as those measured from the present study, as summarised in Table 3.

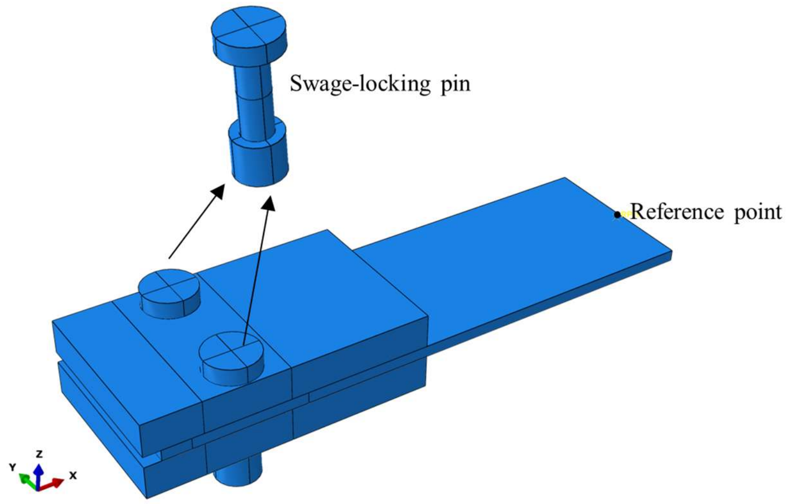

Fig. 7. FE model for swage-locking pinned aluminium alloy shear connection

3.2 Validation

The accuracy of the developed FE models was evaluated by comparing the numerical results including the ultimate resistances, the load-deformation curves and the failure modes with those obtained from the experiments [16]. The ratios of the numerical ultimate resistances (P_{FE}) to the test ultimate resistances (P_{Test}) are reported in Table 5. It can be concluded from Table 5 that the developed FE model can accurately predict the ultimate resistances of swage-locking pinned aluminium alloy shear connections, with the mean value of $F_{\mathrm{FE}}/F_{\mathrm{Test}}$ for all tested specimens being 0.97 and the corresponding COV (coefficient of variation) being 0.039. The numerical and experimental failure modes and load-deformation curves are also compared and illustrated in Figs. 8 and 9 for typical examples, showing good agreement.

Table 5. Comparisons of numerical and experimental [16] ultimate resistances for swage-locking pinned aluminium alloy shear connections

Specimen label	F_{Test} (kN)	F_{FE} (kN)	$F_{\mathrm{FE}}/F_{\mathrm{Test}}$
CS-61-10-50	20.62	19.13	0.93
CS-61-15-50	25.28	24.43	0.97
CS-61-20-50	31.16	29.39	0.94
CS-61-30-50	41.56	40.02	0.96

Specimen label	F_{Test} (kN)	F_{FE} (kN)	$F_{\mathrm{FE}}/F_{\mathrm{Test}}$
CS-61-40-50	50.17	48.63	0.97
CS-63-15-50	19.63	18.52	0.94
CS-63-40-50	38.59	38.41	1.00
CS-82-15-50	26.83	28.77	1.07
CS-82-40-50	52.53	52.51	1.00
CS-04-15-50	34.52	36.48	1.06
CS-04-40-50	66.69	62.66	0.94
CDT-61-30-10-40	54.11	52.80	0.98
CDT-61-30-15-40	67.54	65.66	0.97
CDT-61-30-20-40	80.36	79.62	0.99
CDT-61-30-30-40	81.77	79.26	0.97
CDT-61-30-40-20	60.68	56.87	0.94
CDT-61-30-40-25	64.37	63.10	0.98
CDT-61-30-40-30	73.19	69.17	0.95
CDT-61-30-40-40	85.69	80.27	0.94
CDL-61-30-50-20	63.36	60.43	0.95
CDL-61-30-50-25	67.50	65.31	0.97
CDL-61-30-50-30	75.45	69.11	0.92
CDL-61-30-50-40	84.49	76.57	0.91
Mean			0.97
COV			0.039

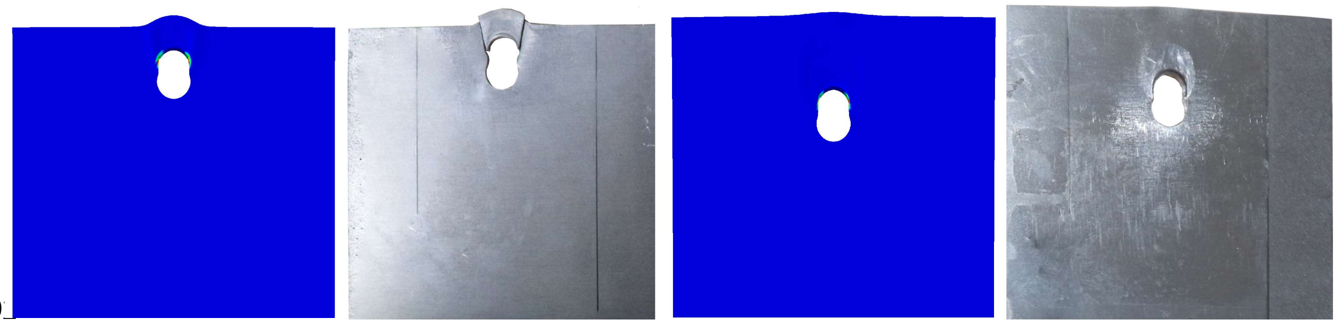

(a) CS-61-15-50 (b) CS-61-30-50

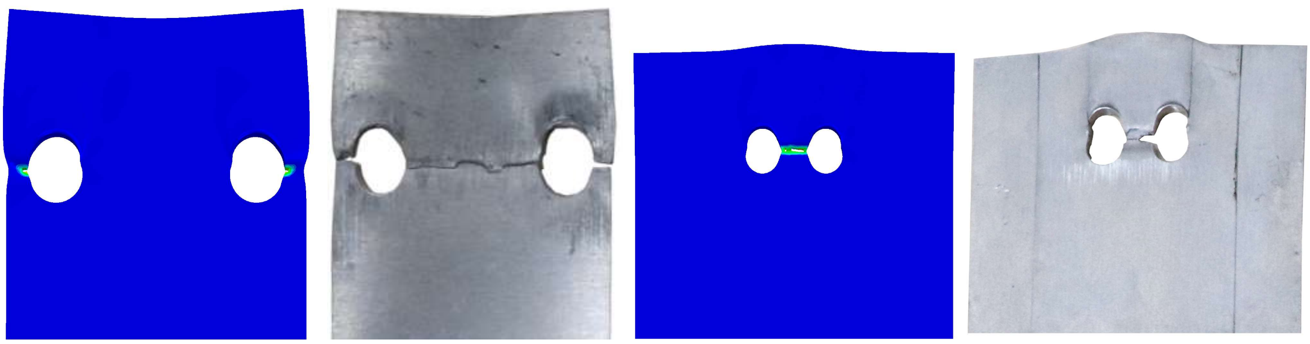

(c) CDT-61-30-10-40 (d) CDT-61-30-40-20

Fig. 8. Comparisons of numerical and experimental failure modes for typical swage-locking pinned aluminium alloy shear connections

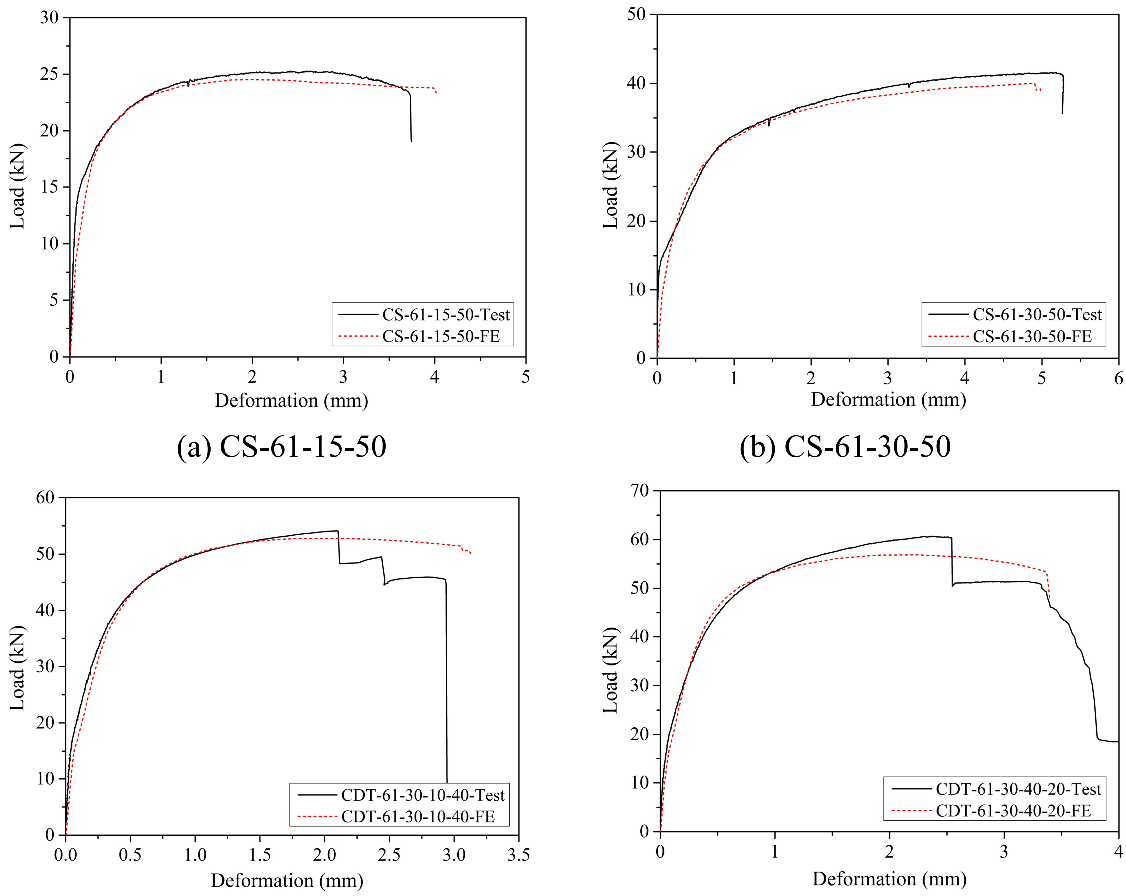

(a) CS-61-15-50 (b) CS-61-30-50

(c) CDT-61-30-10-40 (d) CDT-61-30-40-20

Fig. 9. Comparisons of numerical and experimental load-deformation curves for typical swage-locking pinned aluminium alloy shear connections

4. Parametric studies

4.1 General

Upon validation of the developed FE models, extensive parametric studies were conducted to examine the influence of key parameters, including the friction force, the end distance, the thickness of the inner plate, the pin diameter and the edge distance, on the structural behaviour of swage-locking pinned aluminium alloy shear connections. Four different aluminium alloy grades (i.e. 6061-T6, 6063-T5, 6082-T6 and 7A04-T6) were examined; the stress-strain curves were derived from the Ramberg-Osgood model [40]. The input parameters of the predictive models, including the Young's modulus E, the yield strength (i.e. 0.2% proof stress) $f_{0.2}$ and the ultimate strength f_u, were taken as the measured values reported in Table 1. An efficient computational approach was developed, exploiting ABAQUS interfacing with different programming languages (e.g. Python and Matlab) to automate all the processes (i.e. numerical model creation, job submission and termination and output processing) involved in the parametric studies; the automation strategy helps to facilitate the efficient management of the large amount of numerical analyses in the parametric studies. The results obtained from the parametric studies are discussed in this section and are used as the basis for assessing, and where necessary modifying, the current design equations for swage-locking pinned aluminium alloy shear connections, as presented in Section 5.

4.2 Influence of friction force

As stated in the companion paper [16], the friction between the inner and outer plates contributes to the load-carrying capacity of shear connections. However, the friction force is often difficult to quantify from the experiments, the influence of which is thus investigated numerically in this subsection. The friction force between the inner and outer plates for each aluminium alloy shear connection can be obtained by using the ABAQUS output parameter − the total force due to frictional stress (CFSM). Fig. 10 shows the ratios of the friction forces ($F_{\mathrm{f,FE}}$) and the load-carrying capacities ($F_{\mathrm{u,FE}}$) obtained from ABAQUS models for all the investigated shear connections. It can be seen from Fig. 10 that the friction forces only account for a relatively small percentage, ranging from 14.0% to 27.5%, of the load carrying capacities of aluminium alloy shear connections.

The ratios of $F_{\mathrm{f,FE}}/F_{\mathrm{u,FE}}$ for the shear connections made of the three investigated normal strength aluminium alloys (i.e. 6000 series alloys) are quite close, with the average value of $F_{\mathrm{f,FE}}/F_{\mathrm{u,FE}}$

being 0.25. With regards to the shear connections made of the high strength aluminium alloy (i.e. 7A04-T6), the ratios of $F_{f,FE}/F_{u,FE}$ are generally smaller than those of normal strength aluminium alloys; this may be attributed to the following reasons: (1) the smaller friction coefficient (and thus the smaller friction forces per pin) for 7A04-T6 plates, as indicated in Table 3; and (2) the higher failure load $F_{u,FE}$ of shear connections made of the high strength aluminium alloy, resulting in the friction force being a lower proportion of the specimen failure load (i.e. a lower ratio of $F_{f,FE}/F_{u,FE}$). On the basis of the above findings, it may be concluded that the swage-locking pinned aluminium alloy shear connections may be designed as bearing-type connections provided that the surfaces of the aluminium plates are as-built (not specifically treated). A similar suggestion was also made by Deng et al. [41] based on the studies of single swage-locking pinned aluminium alloy shear connections.

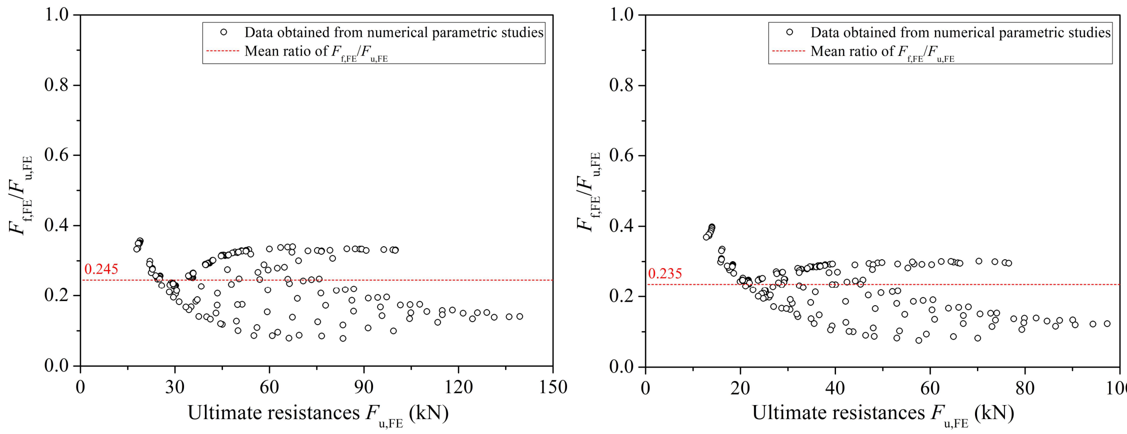

(a) 6061-T6 (b) 6063-T5

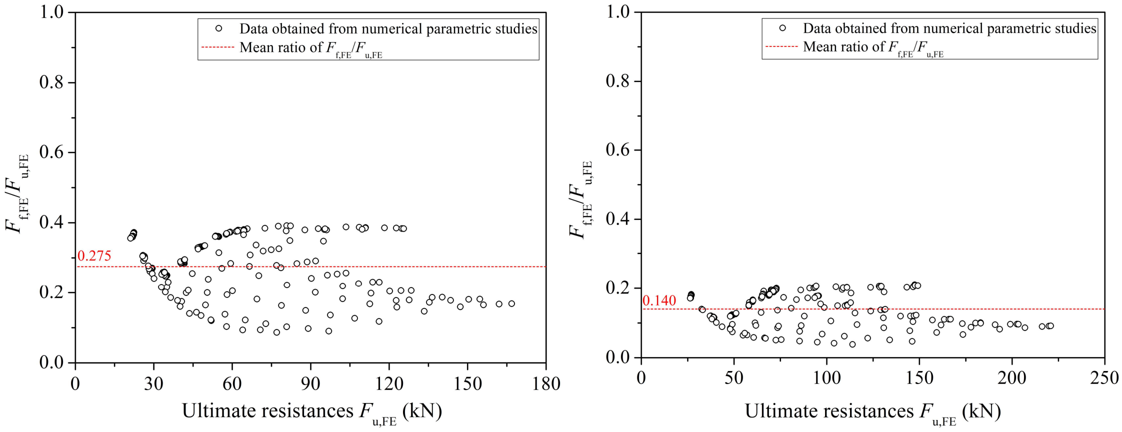

(c) 6082-T6 (d) 7A04-T6

Fig. 10. The friction contribution (at failure load) of aluminium alloy shear connections made of different aluminium alloy grades

To improve the accuracy of the existing design approaches for aluminium alloy shear connections, the friction contribution resulted from preloaded swage-locking pins should be properly accounted for. The friction-deformation histories of typical aluminium alloy shear connections are illustrated in Fig. 11. The specimens in Fig. 11 include shear connections with edge distance of $5.0d_0$ and end distances ranging from $1.0d_0$ to $6.0d_0$ as well as shear connections with edge distance of $1.5d_0$ and end distances ranging from $1.0d_0$ to $5.0d_0$. It can be seen from Fig. 11 that the friction force increases dramatically and almost linearly with the deformation to a peak value where the slippage occurs. After the occurrence of slippage, direct bearing becomes the primary means of the load transfer, leading to a decrease of the friction force for connections with different geometric parameters. For shear connections with large end and edge distances (i.e. $e_1 > 2.5d_0$ and $e_2 = 5.0d_0$), the friction load begins to increase again at a certain deformation (i.e. the inflection point as indicated in Fig. 11) and continues to increase with increasing deformation; the greater the end distance, the faster the friction increases. The increase of the friction force for these shear connections may be attributed to the increase of the preload in swage-locking pins, which results from the material protrusion downstream of the pin hole, as shown in Fig. 12.

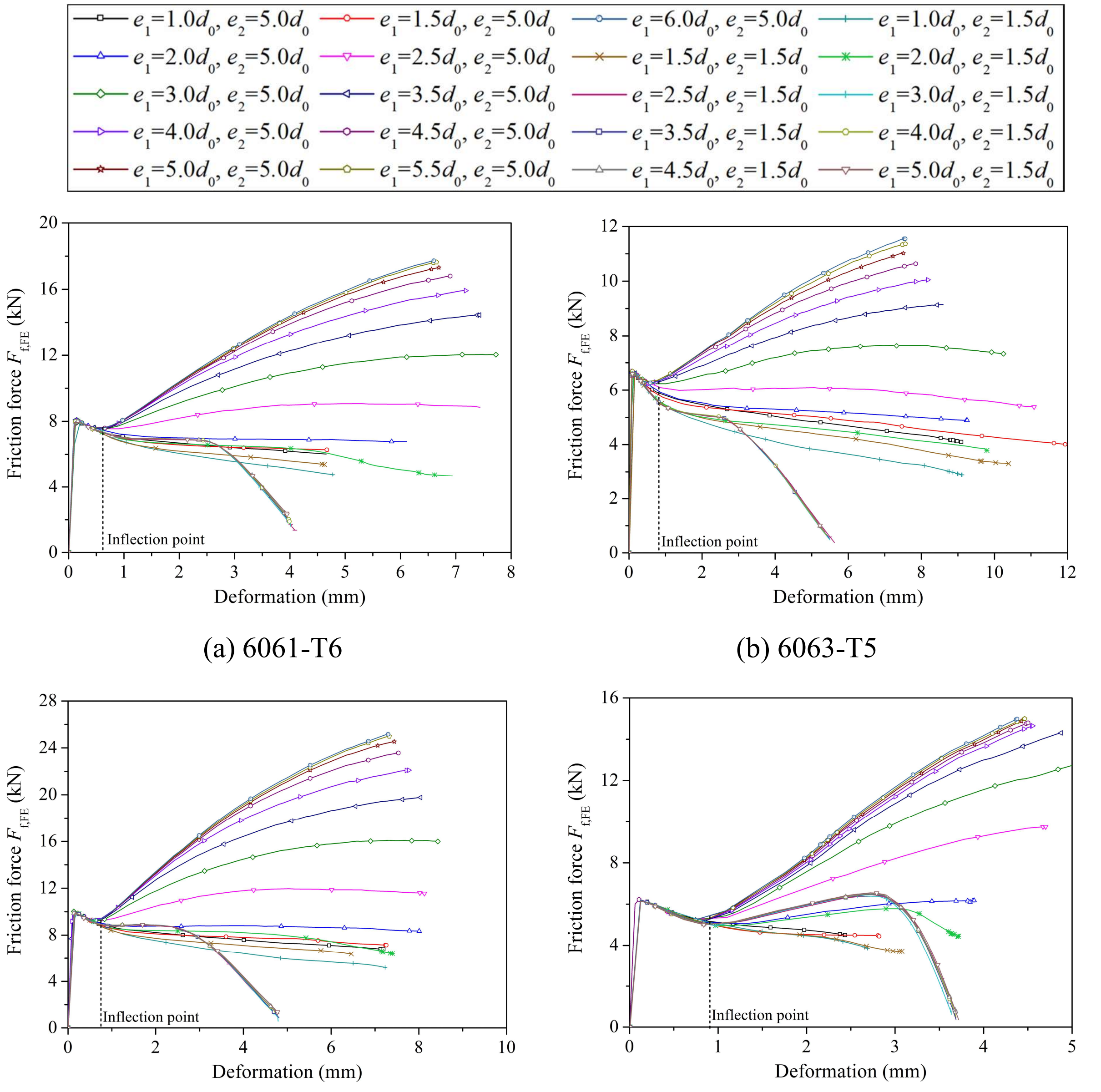

Fig. 11. Friction-deformation histories of shear connections with varied end and edge distances made of different aluminium alloys

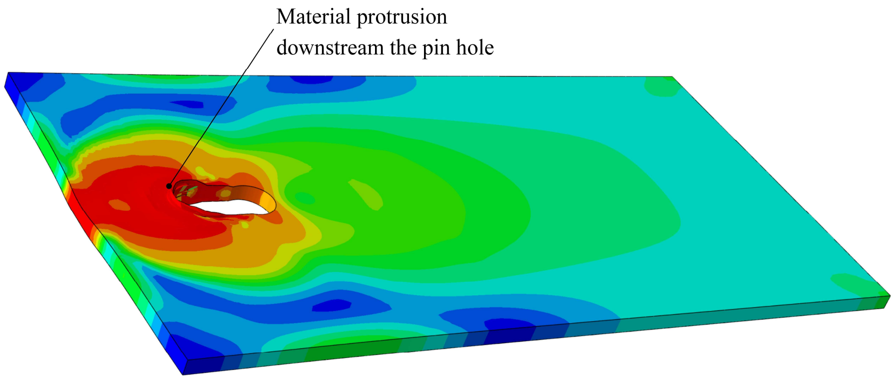

Fig. 12. Material protrusion downstream of the pin hole during loading for connections with large end and edge distances

Considering the above analysis, the resistance of the investigated aluminium alloy shear connections includes two components: the primary resistance from aluminium alloy plates F_p and the friction contribution generated by preloaded swage-locking pins F_fc, as expressed in Eq. (3).

$$F_\mathrm{u} = F_\mathrm{fc} + F_\mathrm{p} \tag{3}$$

The friction contribution generated by preloaded swage-locking pins F_fc can be calculated by Eq. (4) for connections with different geometric parameters,

$$F_\mathrm{fc} = \alpha_\mathrm{fc} \cdot 2n_\mathrm{p} \mu F_\mathrm{p,C} \tag{4}$$

where n_p is the number of the swage-locking pins in the shear connection, $F_\mathrm{p,c}$ is the preload of the swage-locking pin and α_fc is the coefficient of friction contribution. Note that the increased friction load due to the material protrusion downstream of the pin hole is not considered for connections with large end and edge distances, leading to somewhat conservative predictions of F_fc for those connections. The values of α_fc have been calibrated for swage-locking pinned shear connections made of 6061-T6, 6063-T5, 6082-T6 and 7A04-T6 aluminium alloys based on the numerically obtained data of the friction forces. The frictional force values in this study were determined by identifying the inflection point of the frictional force curve, as illustrated in Fig. 11. It is recommended that α_{fc} of 0.90 for normal strength aluminium alloys and 0.83 for high strength aluminium alloys can be applied in Eq. (4) for the determination of friction contribution in aluminium alloy shear connections.

4.3 Influence of end distance ratio

The experiments on aluminium alloy connections with single swage-locking pin [16] showed that for connections made of the same material with the same width b and thickness t, increasing the end distance e_1 led to a failure mode transition from shear-out to bearing. The influence of the end distance e_1 on the response of swage-locking pinned aluminium alloy shear connections is investigated numerically in this subsection. A set of FE models for the double shear configuration with single swage-locking pin, as shown in Type 1 of Fig. 1, was developed with the inner plate thickness of 4 mm and the outer plate thickness of 12 mm. The diameters of the pin d_{pin} and the hole d_0 were set equal to 9.66 mm and 10.5 mm, respectively. The edge distance ratio e_2/d_0 was kept constant at 5.0, while for the end distance ratio e_1/d_0, a total of 11 values (i.e. 1.0, 1.5, 2.0, 2.5, 3.0, 3.5, 4.0, 4.5, 5.0, 5.5 and 6.0) were used. The four different aluminium alloy grades (i.e. 6061-T6, 6063-T5, 6082-T6 and 7A04-T6) were investigated, leading to a total of 44 FE models being investigated.

Fig. 13 shows comparisons between the results obtained for the above mentioned connections. The numerically obtained resistances $F_{u,FE}$ are normalised by the ultimate strength of the material

f_u in Fig. 13(a) since both the ultimate shear-out and bearing resistances of a single-bolt shear connection are found to be proportional to f_u. The normalised ultimate resistances $F_{u,FE}/f_u$ of the 44 numerical specimens are plotted against the end distance ratio e_1/d_0 in Fig. 13(a). It can be seen from Fig. 13(a) that the normalised ultimate resistances of shear connections made of normal strength aluminium alloys (i.e. 6061-T6, 6063-T5 and 6082-T6) increase linearly with the end distance ratio e_1/d_0 until the threshold value of e_1/d_0 (about 3.0) is reached, after which the increasing rate of the normalised ultimate resistances gradually decreases until reaching a constant value at e_1/d_0 approximately equal to 5.0. While for connections made of the high strength aluminium alloy, their normalised ultimate resistances are lower than those made of normal strength aluminium alloys and become nearly constant (still lower than those made of normal strength aluminium alloys) at $e_1/d_0 \approx 3.0$. The lower normalised ultimate resistances for connections made of high strength aluminium alloy 7A04-T6 failing in bearing (i.e. $e_1/d_0 > 3.0$) can be attributed to the lower fracture strain of the high strength aluminium alloy and hence the earlier failure downstream the pin hole of 7A04-T6 plate in bearing, while the lower normalised ultimate resistances for connections made of high strength aluminium alloy 7A04-T6 failing in shear-out (i.e. $e_1/d_0 < 3.0$) may result from the lower friction contribution due to the smaller friction coefficient between 7A04-T6 plates. This is evidenced by Fig. 13(b), where the friction forces $F_{f,FE}$ are eliminated from the ultimate resistances $F_{u,FE}$ before normalising to f_u, and the normalised term of $(F_{u,FE} - F_{f,FE})/f_u$ is plotted against the end distance ratio e_1/d_0. It can be seen from Fig. 13(b) that the results of $(F_{u,FE} - F_{f,FE})/f_u$ for connections made of high strength aluminium alloy 7A04-T6 failing in shear-out (i.e. $e_1/d_0 < 3.0$) coincide with those made of normal strength aluminium alloys, indicating that the material ductility has negligible influence on the shear-out resistances of swage-locking pinned aluminium alloy shear connections. Based on the above discussion, it can thus be concluded that the friction contribution generated by preloaded swage-locking pins should be duly considered in predicting the shear-out resistances of such connections.

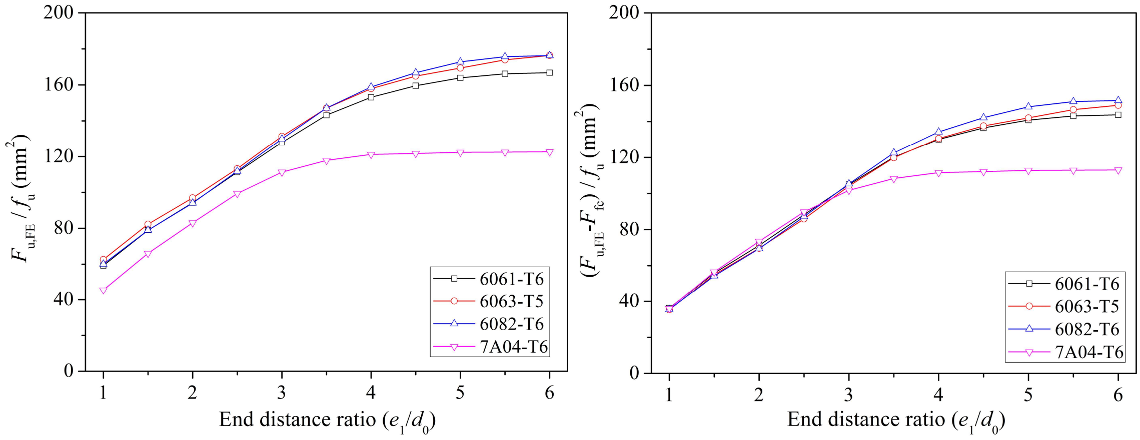

(a) $F_{u,FE}/f_u$ vs. e_1/d_0 (b) $(F_{u,FE} - F_{f,FE})/f_u$ vs. e_1/d_0

Fig. 13. The influence of end distance on the resistances of swage-locking pinned aluminium alloy shear connections

4.4 Influence of inner-plate thickness

A series of parametric studies on connections with single swage-locking pin in double shear and inner plate thicknesses ranging from 4 mm to 12 mm with 1 mm interval were investigated. The arrangement of the FE models is shown in Type 1 of Fig. 1. The diameters of the pin d_{pin} and the hole d_0 were set equal to 9.66 mm and 10.5 mm, respectively. The edge distance ratio e_2/d_0 was kept constant at 5.0, while for the end distance ratio e_1/d_0, a total of 9 values (i.e. 1.0, 1.5, 2.0, 2.5, 3.0, 3.5, 4.0, 4.5 and 5.0) were used. The four different aluminium alloy grades (i.e. 6061-T6, 6063-T5, 6082-T6 and 7A04-T6) were investigated, leading to a total of 324 FE models being investigated in this subsection. For connections with the inner plate thickness smaller than or equal to 10 mm, the outer plate thickness of 12 mm was used, while for connections with a thicker inner plate thickness of 11 mm or 12 mm, the outer plate thickness was increased to 16 mm to ensure that failure and the associated deformations were concentrated in the inner aluminium alloy plates. The results of the parametric studies are shown in Fig. 14, where the ultimate resistances of the investigated swage-locking pinned aluminium alloy shear connections are plotted against their corresponding inner plate thicknesses.

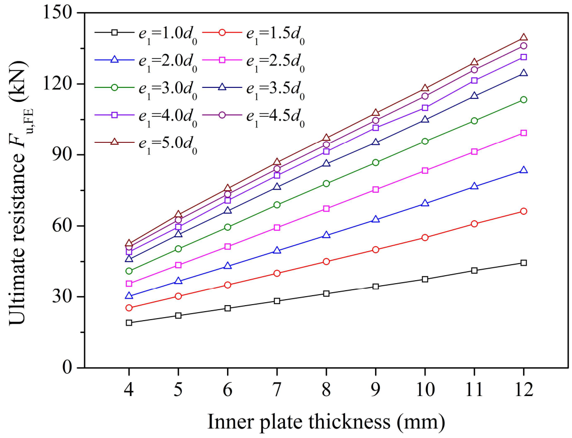

(a) 6061-T6

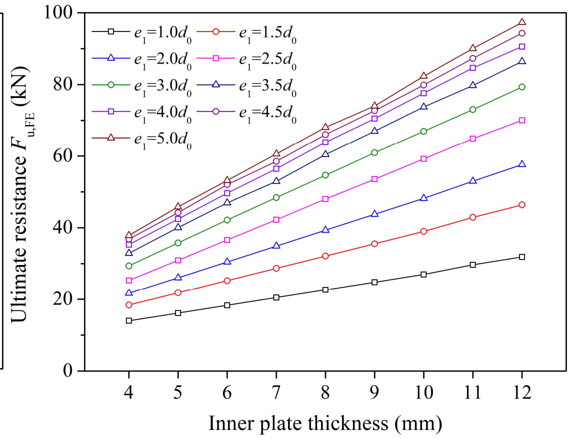

(b) 6063-T5

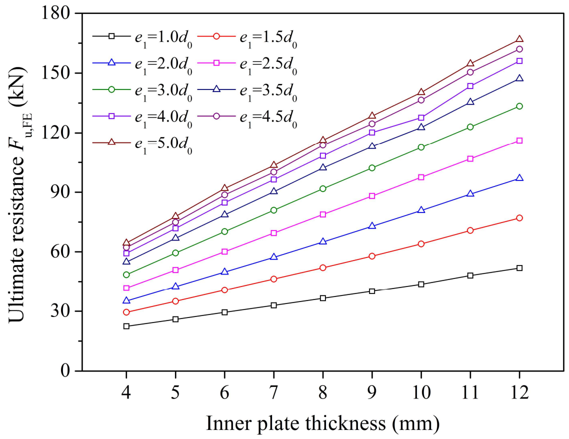

(c) 6082-T6

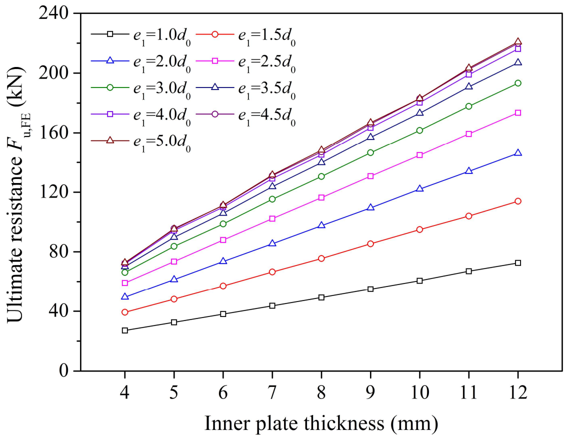

(d) 7A04-T6

Fig. 14. The influence of inner plate thickness on the ultimate resistances of swage-locking pinned aluminium alloy shear connections

It can be seen from Fig. 14 that, for the investigated swage-locking pinned aluminium alloy shear connections with different aluminium alloy grades and end distance ratios, the ultimate resistances increase linearly with increasing value of the inner plate thicknesses. It can also be observed from Fig. 14 that for swage-locking pinned aluminium alloy shear connections made of 7A04-T6 and with the same inner plate thickness, their ultimate resistances barely increase when the end distance ratio e_1/d_0 is greater than 3.0, which confirms the conclusion drawn in Subsection 4.3.

4.5 Influence of pin diameter

The influence of the pin diameter d_{pin} on the ultimate resistances of swage-locking pinned aluminium alloy shear connections is investigated in this subsection. Since the granularity of the diameter of commonly used swage-locking pins is 1/16 inch, six pin diameters of 9.66 mm (6/16 inch), 12.70 mm (8/16 inch), 15.88 mm (10/16 inch), 19.05 mm (12/16 inch) and 22.23 mm (14/16 inch) were selected in the parametric studies. The diameter of the pin hole was set as 1 mm larger than the nominal pin diameter d_{pin} and rounded to the nearest 0.5 mm. It has been found in [43] that the ultimate resistances of shear connections are influenced by the pin diameter d_{pin}, while the hole diameter is considered to have negligible influence; therefor the parameter of the hole diameter was not considered in the parametric studies. Different end distances and alloy types as those in Section 4.4 were also considered herein, while the thicknesses of the inner and outer plates of the shear connections were set equal to 4 mm and 12 mm, respectively. The influence of the pin diameter on the ultimate resistance of swage-locking pinned aluminium alloy shear connections is illustrated in Fig. 15, where a linear relationship between the pin diameter d_{pin} and the resistance of the connections with the same end distance ratio was identified.

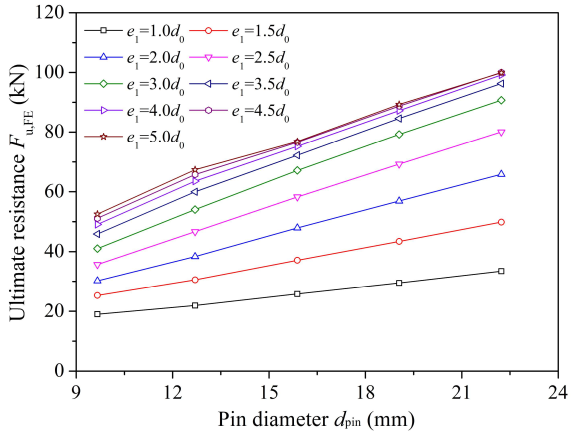

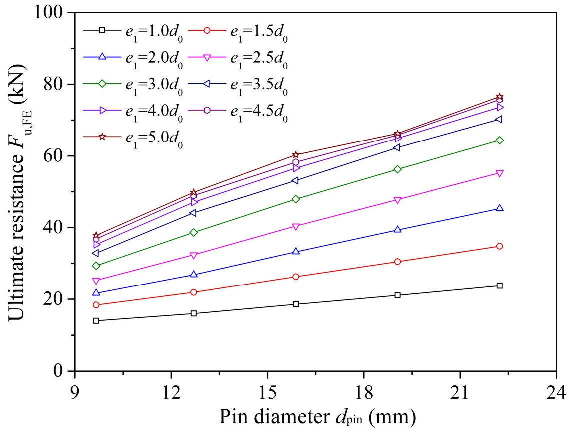

(a) 6061-T6 (b) 6063-T5

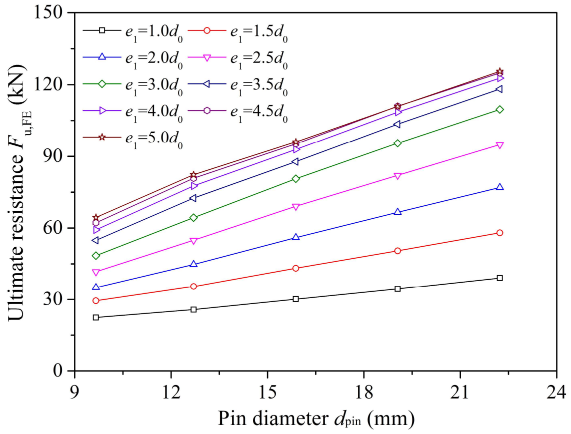

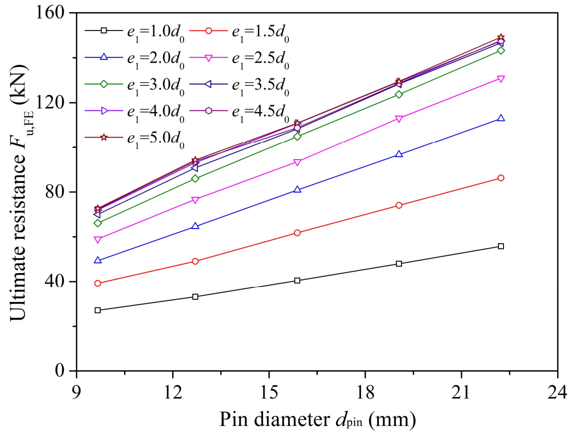

(c) 6082-T6 (d) 7A04-T6

Fig. 15. The influence of pin diameter on the ultimate resistances of swage-locking pinned aluminium alloy shear connections

4.6 Influence of edge distance ratio

A total of 360 numerical simulations were performed to investigate the influence of the edge distance ratio e_2/d_0 on the ultimate resistances of aluminium alloy connections with single swage-locking pin in double shear. The inner plate and outer plate thicknesses of the modelled specimens were kept constant at 4 mm and 12 mm, respectively, while the diameters of the pin d_{pin} and the hole d_0 were set equal to 9.66 mm and 10.5 mm, respectively. For FE models with the same edge distance ratio e_2/d_0, nine end distance ratios e_1/d_0 ranging from 1.0 to 5.0 with 0.5 intervals were considered. The ultimate resistances of swage-locking pinned aluminium alloy shear connections obtained from the parametric studies are grouped by the edge distance ratio e_2/d_0, and plotted against the end distance ratio e_1/d_0 in Fig. 16.

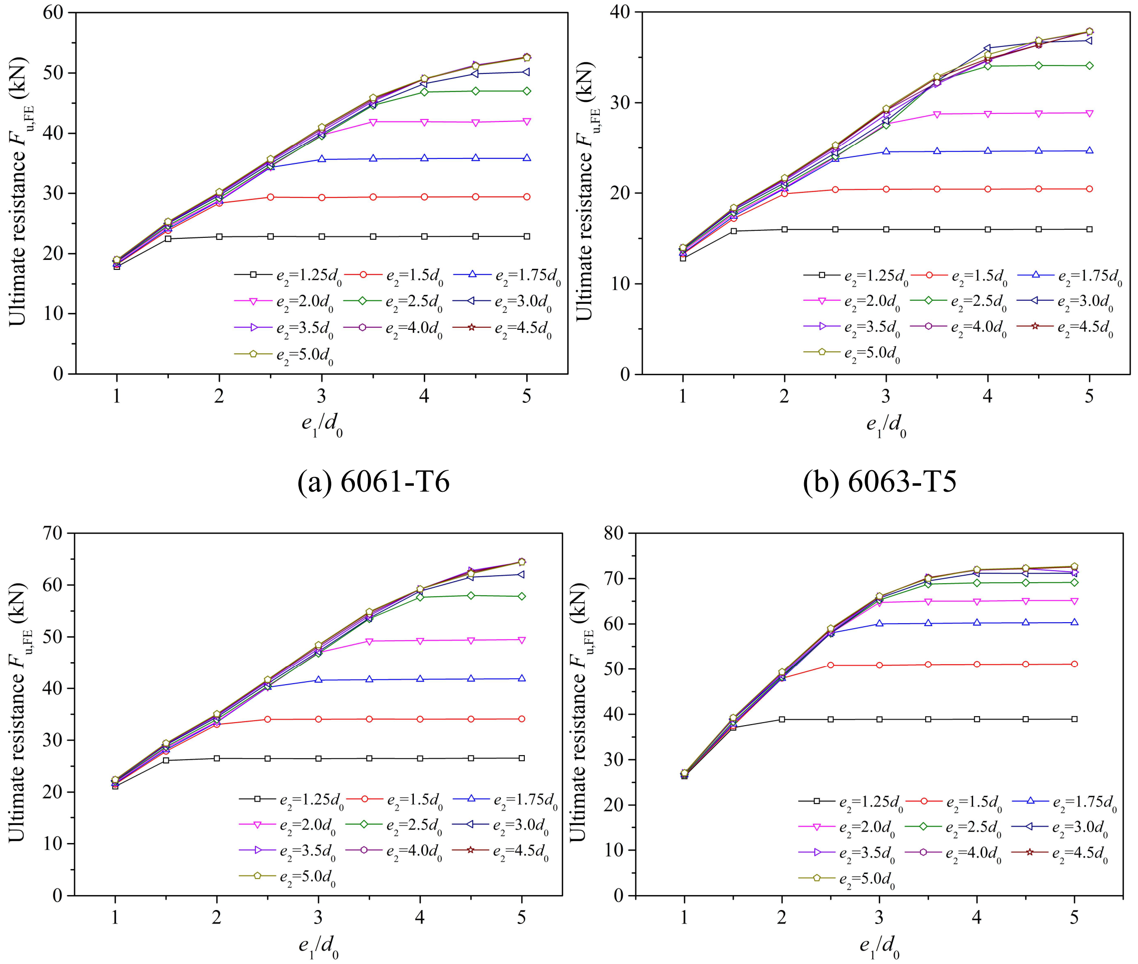

(a) 6061-T6 (b) 6063-T5

(c) 6082-T6 (d) 7A04-T6

Fig. 16. The influence of edge distance ratio on the ultimate resistances of swage-locking pinned aluminium alloy shear connections

It can be seen from Fig. 16 that for connections made of the same aluminium alloy with the same edge distance ratio e_2/d_0, their ultimate resistances trend to increase with increasing end distance ratio e_1/d_0 until reaching an almost constant peak value at a threshold end distance ratio e_1/d_0. The threshold end distance ratio e_1/d_0 is shown to decrease with reducing edge distance ratio e_2/d_0. For connections with relatively large edge distance ratios e_2/d_0 (i.e. $e_2/d_0 \geq 3.0$), the increasing of the edge distance ratio e_2/d_0 fails to result in any improvement in their ultimate resistances, as shown in Fig. 16. Three-dimensional diagrams are shown in Fig. 17 to reveal the coupled influence of the edge distance ratio e_2/d_0 and end distance ratio e_1/d_0 on the ultimate resistances of swage-locking pinned aluminium alloy shear connections, reflecting the observations made above.

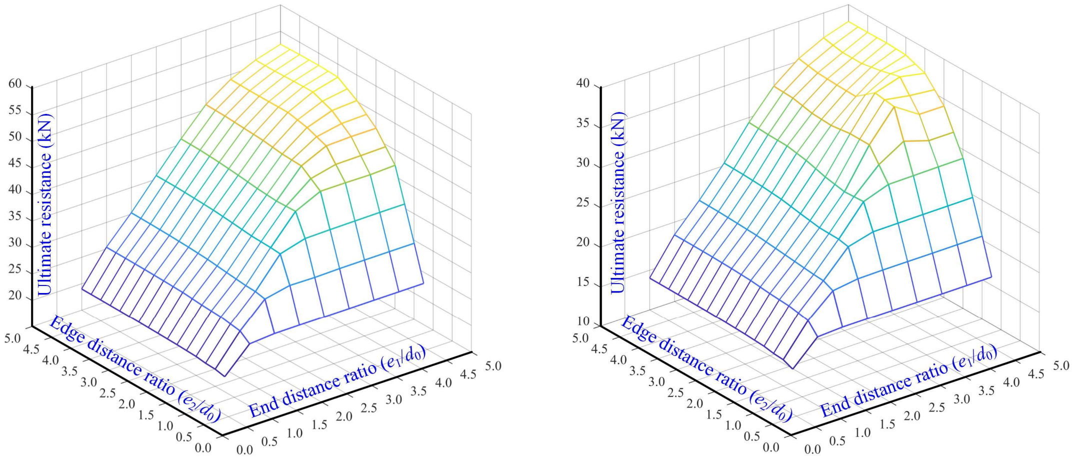

(a) 6061-T6 (b) 6063-T5

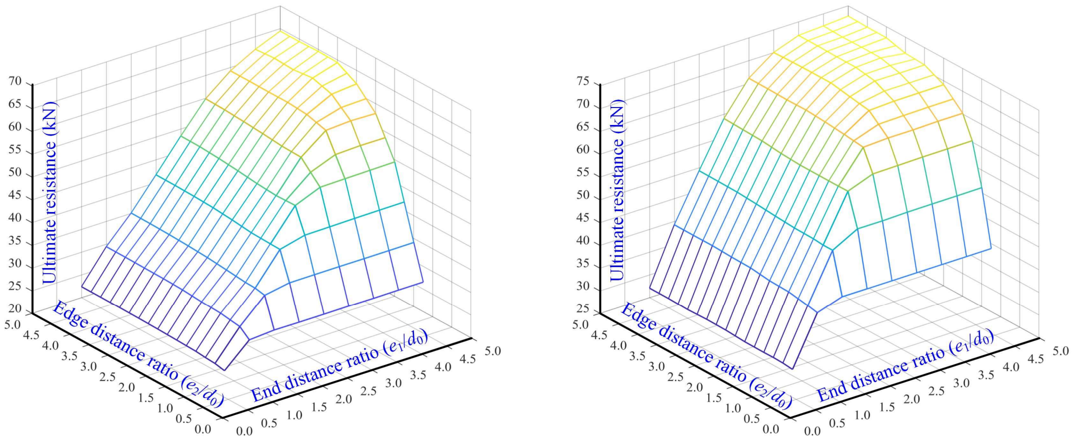

(c) 6082-T6 (d) 7A04-T6

Fig. 17. The coupled influence of edge distance and end distance ratios on the ultimate resistances of swage-locking pinned aluminium alloy shear connections

5. Design recommendations

From the existing test data on swage-locking pinned aluminium alloy shear connections [16], it has been observed that the current design methods can be rather conservative for predicting the resistances of these shear connections failing in bearing or shear-out. In this section, new design recommendations have been made for swage-locking pinned aluminium alloy shear connections on the basis of the experimental and numerical results.

5.1 Design equations for shear-out resistance

When the shear-out failure mode governs the ultimate resistance of the connection, the material downstream of the pin hole reaches the ultimate shear strength [44] and the shear length L_v is critical in determining the shear-out resistances. Different definitions of the shear length L_v have been made, namely (1) the gross shear length L_{gv}[45], (2) the net shear length L_{nv} [46] and (3) the active shear length L_{av}, as graphically illustrated in Figs. 18 (a)-(c) respectively. The active shear length L_{av} is assumed to be equal to the average value of the gross shear length L_{gv} and the net shear length L_{nv}. This assumption was proposed by [44] and has been verified by a number of studies on bolted steel shear connections [47-49], but the location of the active shear plane requires modification for applicability to the particularly investigated swage-locking pinned aluminium alloy shear connections.

The following equation is proposed for the prediction of the ultimate shear-out resistances of swage-locking pinned aluminium alloy shear connections:

$$F_{SO} = 1.2 L_{pv} t f_u + F_{fc} \tag{5}$$

where F_{fc} is the friction contribution generated by preloaded swage-locking pins, and L_{pv} is the practical shear length which can be expressed in terms of a proportionality coefficient k_{pv} and the end distance e_1, as given by Eq. (6). The proportionality coefficient k_{pv} was calibrated based on a large set of numerical data by means of regression analysis, as shown in Fig. 19. Good agreement can be seen between the numerical data points and the fitted line, with the parameter k_{pv} taken equal to 0.74. Substituting Eq. (6) into Eq. (5) leads to the proposed equation (i.e. Eq. (7)) for swage-locking pinned aluminium alloy shear connections failing in shear-out failure.

$$L_{pv} = k_{pv} e_1 \tag{6}$$

$$F_{SO,Rd} = 0.89 e_1 t f_u + F_{fc} \tag{7}$$

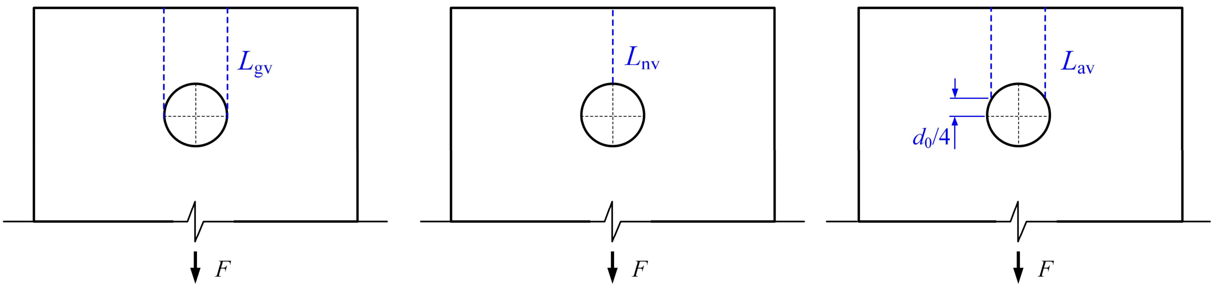

(a) Gross shear length (b) Net shear length (c) Active shear length

Fig. 18. Different definitions of shear lengths

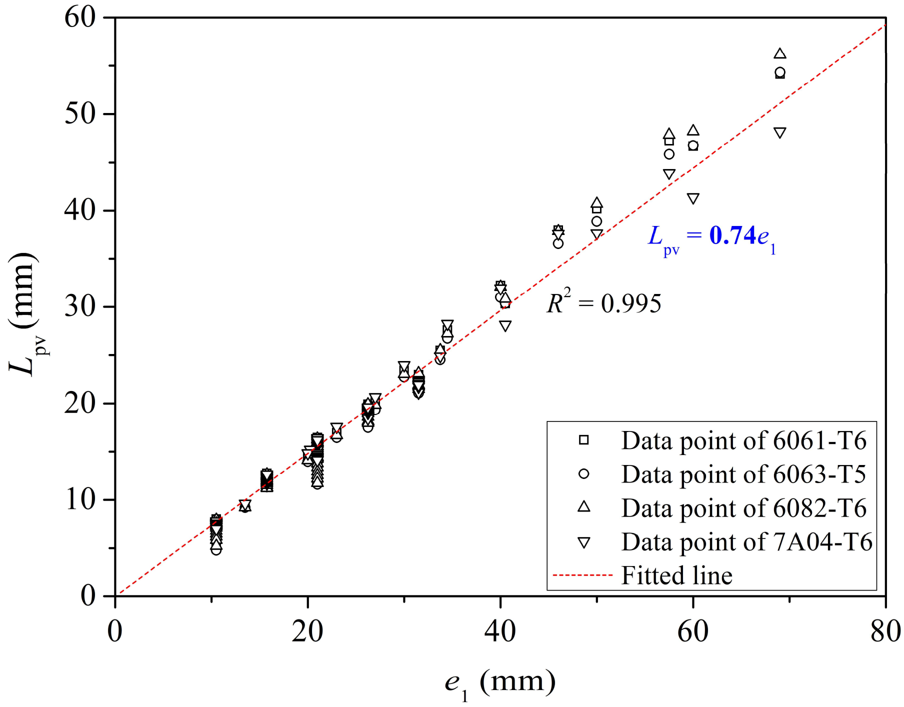

Fig. 19. Calibration of k_{pv} based on a total of 379 numerical parametric data

The experimental and numerical results ($F_{SO,test/FE}$) were utilised to assess the accuracy of the proposed design equation (Eq. (6)), as well as those specified in European (EC9) [18], American (AA 2015) [7] and Australian/Zelanian (AS/NZS 1664.1:1997) [19]. Since the Chinese code [20] does not allow the use of shear connections with end distance smaller than $2d_0$, it was not assessed and compared with other design specifications herein. Detailed information regarding the design equations for the bearing and shear-out resistances of aluminium alloy connections specified in different design specifications can be found in Section 3.3 of Reference [16]. Note that as the current codified design methods [18-19] do not explicitly account for the friction contribution F_{fc}, the experimentally and numerically obtained resistances with the F_{fc} excluded were employed and compared with the predicted resistances according to the three codified design methods, as shown in Figs. 20 (a)-(c). The experimental and numerical resistances without and with the F_{fc} were compared with the proposed design approach, as shown in Figs. 20 (d) and (e), respectively. Key statistical values, including the mean and COV of the predicted-to-test/FE results, determined using different design approaches, are summarised in Table 6.

It can be seen from Fig. 20 (a) and Table 6 that, despite a relatively low level of scatter, the EC9 [18] predictions are generally conservative due to the adoption of a smaller proportionality coefficient for shear length (i.e. equivalent to 0.69, however this coefficient is not explicitly expressed in EC9 [18]) than the calibrated value of k_{pv} in the proposed Eq. (6)). The mean value of $F_{SO,AA}/F_{SO,test/FE}$ is very close to unity, but the design provisions in AA 2015 [7] overestimate the resistances of shear connections with small e_1 while underestimate those with large e_1, hence yielding a high degree of scatter in the prediction of shear-out resistances. The shear-out design equation specified in in AS/NZS 1664.1:1997 [19] is quite similar to that set out in AA 2015 [7], except for a lower upper limit on the bearing stress [16], leading to more conservative predictions $F_{SO,AS/NZS}$ compared to those of $F_{SO,AA}$. Compared to the current codified design equations, the proposed design equations (i.e. Eq. (6) and Eq. (7) for shear out resistances with and without consideration of the friction contribution) yield much more accurate and less scattered resistance predictions, despite the friction contribution is considered or not.

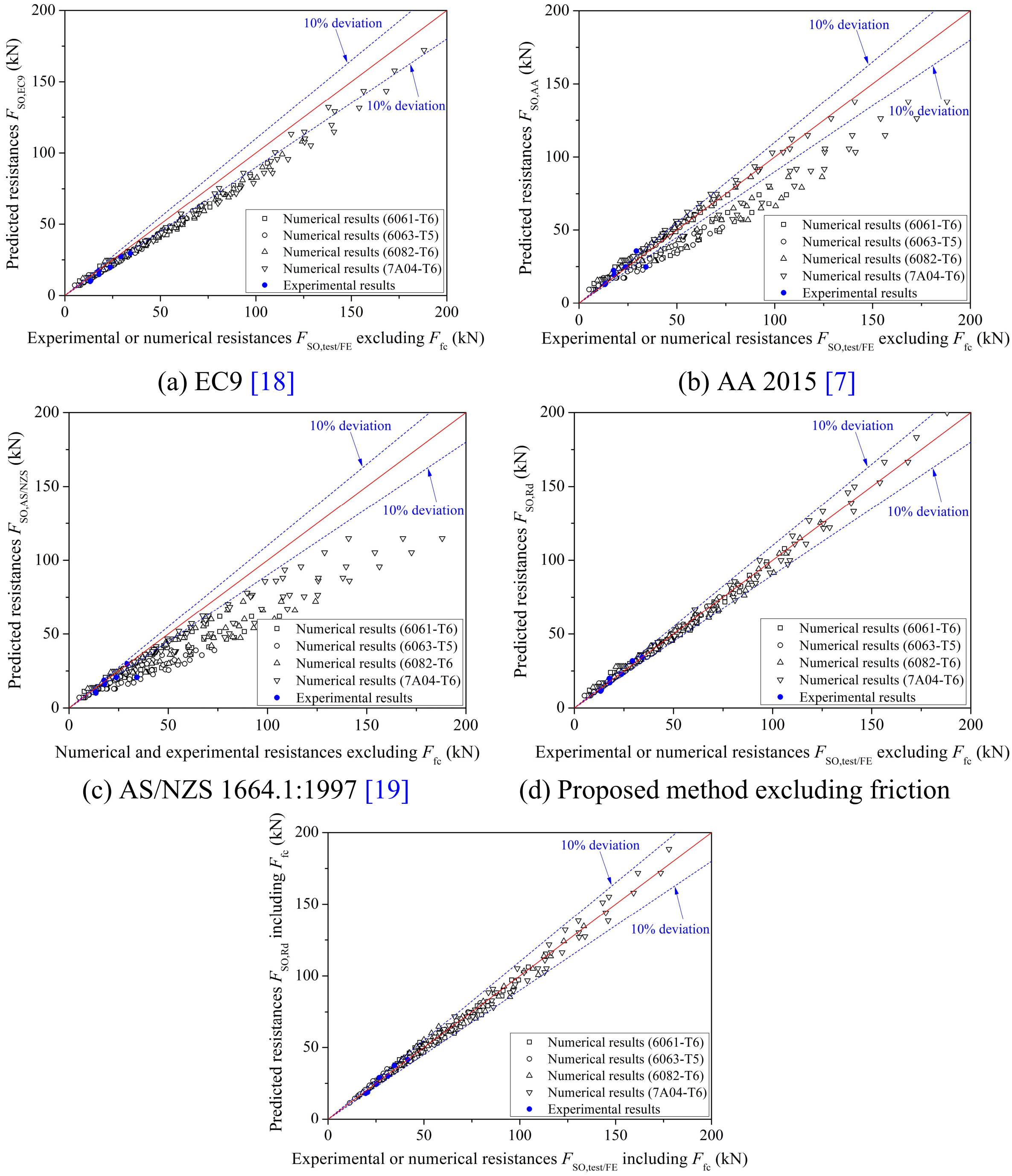

(a) EC9 [18]

(b) AA 2015 [7]

(c) AS/NZS 1664.1:1997 [19]

(d) Proposed method excluding friction

(e) Proposed method including friction

Fig. 20. Comparison of experimental and numerical results with resistance predictions from different design methods for shear-out failure mode

Table 6. Assessment of different design methods for aluminium shear connections failing by shear-out

	$F_{SO,pred}/(F_{SO,test/FE} - F_{fc})$				$F_{SO,pred}/F_{SO,test/FE}$
	EC9	AA 2015	AS/NZS	Proposed method	Proposed method
Mean	0.89	1.01	0.82	1.03	1.01
COV	0.083	0.19	0.20	0.085	0.045

5.2 Design equations for bearing resistance

Current codified equations for calculating the bearing resistances of shear connections follow the same basic format, as given by Eq. (8):

$$F_B = C_B d_{pin} t f_u \tag{8}$$

where C_B is the bearing coefficient. For bolted connections made of less ductile metal materials, such as cold-reduced steel [50] and high strength aluminium alloy (i.e. 7A04-T6), their bearing resistances remain approximately constant with increasing end distance ratio (see Fig. 13), hence C_B can be taken as a constant value. However, for bolted connections made of ductile metal materials such as stainless steel [51] and the normal strength aluminium alloy (i.e. 6061-T6, 6063-T5 and 6082-T6), their bearing resistances generally increase with increasing end distance ratio; C_B can therefore be expressed in terms of the end distance ratio to reflect this observation. The current paper adopts the format of Eq. (8) for determining the bearing resistances of swage-locking pinned aluminium alloy shear connections, with the bearing coefficient C_B calibrated based on the experimentally and numerically obtained data on connections with $e_1 \geq 3.0d_0$ that are governed by bearing failure. The proposed bearing resistance design expressions are given by Eqs. (9a) and (9b) for swage-locking pinned shear connections made of normal strength aluminium alloy (i.e. 6061-T6, 6063-T5 and 6082-T6) and high-strength aluminium alloy (i.e. 7A04-T6), respectively,

$$F_{\mathrm{B,Rd}} = C_{\mathrm{B,NSA}} d_{\mathrm{pin}} t f_{\mathrm{u}} + F_{\mathrm{fc}} \quad \text{for normal strength aluminium alloy} \tag{9a}$$

$$F_{\mathrm{B,Rd}} = C_{\mathrm{B,HSA}} d_{\mathrm{pin}} t f_{\mathrm{u}} + F_{\mathrm{fc}} \quad \text{for high strength aluminium alloy} \tag{9b}$$

in which $C_{\mathrm{B,NSA}}$ and $C_{\mathrm{B,HSA}}$ are the proposed bearing coefficients for normal and high strength aluminium alloys, respectively:

$$C_{\mathrm{B,NSA}} = \min\,[0.52(e_1/d_0) + 1.28,\ 3.62] \quad \text{for } e_1/d_0 \geq 3.0,\ e_2/d_0 > 3.0 \tag{10a}$$

$$C_{\mathrm{B,HSA}} = 2.83 \quad \text{for } e_1/d_0 \geq 3.0,\ e_2/d_0 > 3.0 \tag{10b}$$

The accuracy of the bearing coefficients employed in different design standards and those adopted in proposed design approaches by Teh et al.[42], Zhang [43] and the authors is assessed by comparisons against experimental and numerical data, as shown in Fig. 21. A bearing coefficient C_{B} of 3.5 was employed in Teh's proposal [42] while Zhang [43] suggested the use of the following equation for determining C_{B} for aluminium alloy shear connections:

$$C_{\mathrm{B}} = 0.85(e_1/d_0) + 0.5 \text{ but} \leq 3.9 \tag{11}$$

It can be seen from Fig. 21 that all the codified design methods underestimate to different extents the bearing resistances of the investigated swage-locking pinned aluminium alloy shear connections. The Teh's proposal [42] provides more accurate predictions for normal strength aluminium alloy shear connections than the codified design methods, however, yields predictions on the unsafe side for high strength aluminium alloy specimens. The design approach proposed by Zhang [43] generally overestimates the bearing coefficient of shear connections made of both normal and high strength aluminium alloys. The proposed bearing coefficient in the current paper provides better agreement with the experimental and numerical data in comparison to existing design methods. The comparisons of test and FE bearing resistances with those predicted by different design methods are summarised in Table 7, confirming the improved accuracy of the proposed method. It should be noted that the proposed equations (Eqs. (9a) and (9b)) also ensure a continuous transition from the shear-out and bearing resistance predictions for specimens with a threshold end distance ratio of 3.0.

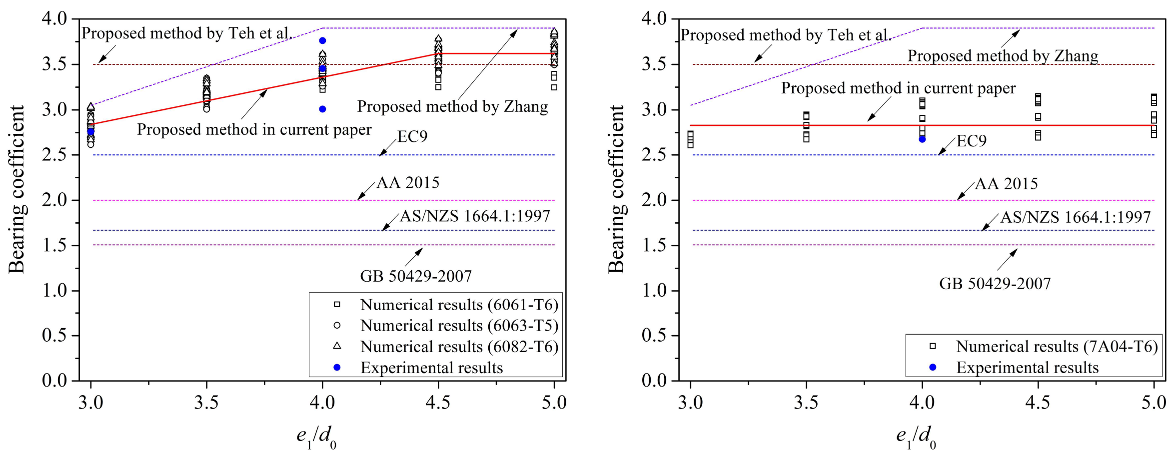

(a) Normal strength aluminium alloys (b) High strength aluminium alloy

Fig. 21. Assessment of the accuracy of different bearing coefficients employed in codified and proposed design methods

Table 7. Assessment of different design methods for aluminium shear connections failing by bearing

Aluminium alloy		$F_{B,pred}/(F_{B,test/FE} - F_{fc})$							$F_{B,pred}/F_{B,test/F}$
		EC9 [18]	AA 2015 [7]	AS/NZS [19]	GB [20]	Teh et al. [42]	Zhang [43]	Proposed method	Proposed method
Normal strength	Mean	0.76	0.61	0.49	0.46	1.07	1.17	1.00	1.00
	COV	0.076	0.061	0.054	0.046	0.110	0.091	0.035	0.031
High strength	Mean	0.87	0.69	0.58	0.52	1.21	1.35	0.98	0.98
	COV	0.050	0.040	0.033	0.030	0.070	0.170	0.056	0.054

5.3 Shear out and bearing resistances considering the effect of edge distances

As shown from Fig. 22, the shear-out and bearing resistances of swage-locking pinned aluminium alloy shear connections are influenced by the edge distance ratio e_2/d_0, especially for connections with $e_2/d_0 \leq 3.0$.

To take due account of the influence of edge distance ratio e_2/d_0 on the shear out and bearing resistances of swage-locking pinned aluminium alloy shear connections, an additional coefficient C_E was proposed in the determination of the shear connection resistances $F_{SO/B,Rd}$, as given by Eq. (12):

$$F_{SO/B,Rd} = \min\left(C_E d_{pin} t f_u + F_{fc}, F_{SO,Rd}, F_{B,Rd}\right) \tag{12}$$

The coefficient C_E was calibrated based on the experimentally and numerically obtained data on shear connections with edge distance ratios $e_2/d_0 \leq 3.0$, as given in Eqs. (13a) and (13b) for connections made of normal ($C_{E,NSA}$) and high ($C_{E,HSA}$) strength aluminium alloys, respectively.

$$C_{\mathrm{E,NSA}} = 4.24 - 9.63 \times 0.40^{(e_2/d_0)} \tag{13a}$$

$$C_{\mathrm{E,HSA}} = 2.86 - 17.86 \times 0.13^{(e_2/d_0)} \tag{13b}$$

The accuracy of the further improved method (i.e. Eq. (12)) that accounts for the influence of edge distance ratio e_2/d_0 is assessed by comparisons against test and FE data, as shown in Fig. 22. The accuracy of the design approach in EC9 [18], being the only codified method that considers the influence of edge distance ratio e_2/d_0, has also been evaluated in Fig. 22. It can be seen from Fig. 22 that the EC9 method leads to an overestimation of the ultimate resistances of shear connections with $e_2/d_0 \leq 1.75$. The proposed design method (i.e. Eq. (12)) can provide more accurate and less scattered resistance predictions for swage-locking pinned aluminium alloy shear connections with edge distances $e_2/d_0 \leq 3.0$ than the EC9 method.

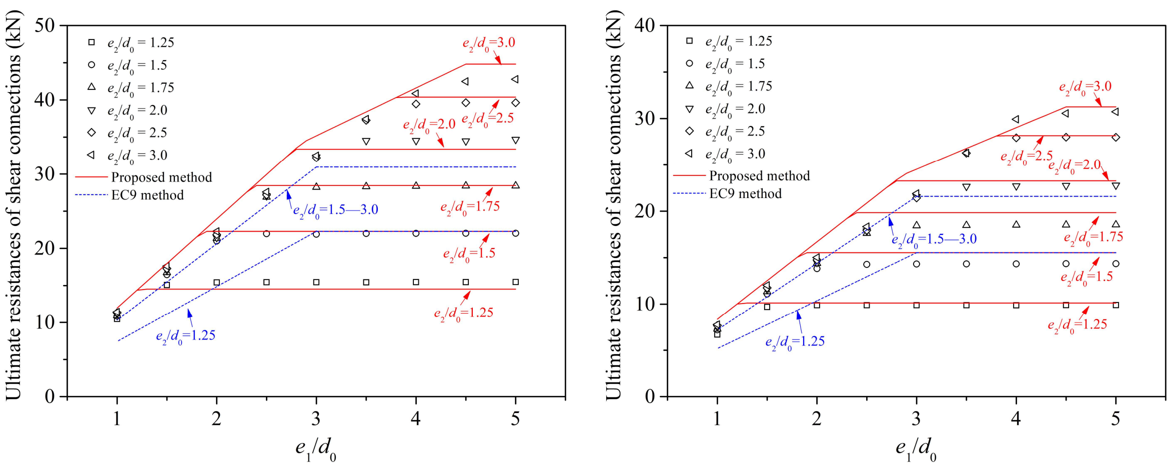

(a) 6061-T6 specimens (b) 6063-T5 specimens

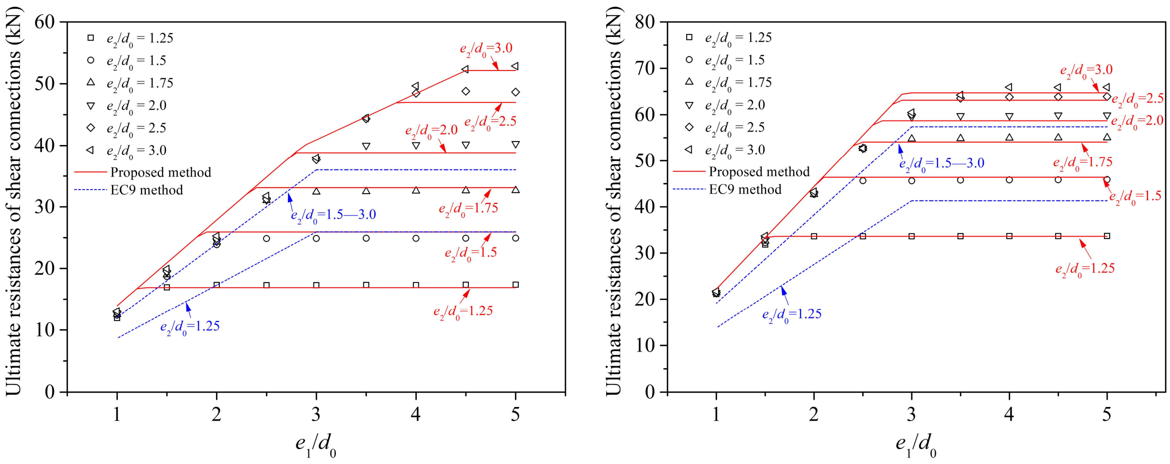

(c) 6082-T6 specimens (d) 7A04-T6 specimens

Fig. 22. Assessment of the accuracy of Eq. (12) and EC9 for determining the ultimate resistances of swage-locking pinned aluminium alloy shear connection with $e_2/d_0 \leq 3.0$ considering the effect of edge distance ratio.

5.4 Design equations for net section and block shear resistances

It has been shown from the previous study [16] that the existing design provisions offer somewhat conservative predictions for net section and block shear resistances of the investigated aluminium alloy connections, primarily due to the lack of consideration of the friction contribution generated by preloaded swage-locking pins. The friction contribution is now properly considered by adding the predicted F_{fc} (Eq. (4)) to the EC9 equations for determining the net section ($F_{NS,Rd}$) and block shear ($F_{BS,Rd}$) resistances, as shown in Eqs. (14) and (15), respectively,

$$F_{\mathrm{NS,Rd}} = 0.9 A_{\mathrm{n}} f_{\mathrm{u}} + F_{\mathrm{fc}} \tag{14}$$

$$F_{\mathrm{BS,Rd}} = \frac{\sqrt{3}}{3} f_{0.2} A_{\mathrm{nv}} + f_{\mathrm{u}} A_{\mathrm{nt}} + F_{\mathrm{fc}} \tag{15}$$

in which A_n is the net section area, A_{nv} is the net area in shear and A_{nt} is the net area in tension. The experimental results F_{test} [16]

were utilised to assess the accuracy of the proposed equations (i.e. Eqs. (14) and (15)) in determining the net section ($F_{NS,Rd}$) and block shear ($F_{BS,Rd}$) resistances, as summarised in Table 8, in which $F_{NS/BS,EC9}$ and $F_{NS/BS,Rd}$ are the predicted results by EC9 and the proposed equations (i.e. Eqs. (14) and (15)), respectively. It can be seen from Table 8 that the proposed equations considering the friction contribution can result in improved predictions on the net section and block shear resistances of swage-locking pinned aluminium alloy shear connections with the mean value of $F_{NS,BS/Rd}/F_{test}$ being 1.02 and the COV being 0.051.

Table 8. Comparison of test results [16] with predicted resistances by Eqs. (14) and (15) for net section and block shear failure

Specimen	F_{test} (kN)	$F_{NS,BS/EC9}/F_{test}$	$F_{NS,BS/Rd}/F_{test}$
CDT-61-30-10-40 (NS)	54.1	0.42	1.11
CDT-61-30-15-40 (NS)	67.5	0.80	1.06
CDT-61-30-20-40 (NS)	80.4	0.73	1.03
CDT-61-30-30-40 (BS)	81.8	0.72	1.03
CDT-61-30-40-20 (BS)	60.7	0.72	0.96
CDT-61-30-40-25 (BS)	64.4	0.77	1.00
CDT-61-30-40-30 (BS)	73.2	0.77	0.97
CDT-61-30-40-40 (BS)	85.7	0.69	0.98
Mean		0.70	1.02
COV		0.170	0.051

6. Conclusions

Finite element models simulating the behaviour of swage-locking pinned aluminium alloy shear connections with various geometric configurations and aluminium alloy grades were developed and validated against experimental data reported in the literature [16]. Prior to the establishment of FE models, measurements on the preloads of swage-locking pins and slip coefficients between aluminium alloy plates were conducted, and these measurements were carefully employed in the developed FE models for validation purposes. Following successful validation, a series of parametric studies, with over 900 additional numerical data being created, were carried out to investigate the influence of several key parameters including the friction force, the end distance, the thickness of the inner plate, the pin diameter and the edge distance on the failure mode and resistance of the studied aluminium alloy shear connections. On the basis of the large amount of structural performance data, the friction contribution generated by preloaded swage-locking pins on the ultimate resistances of the investigated shear connections was quantified and the prediction equations have been proposed. In addition, improved design equations for determining the shear-out and bearing resistances of swage-locking pinned aluminium alloy shear connections, considering the friction contribution and the effect of edge distance ratio, were proposed, which have been shown to result in more accurate and less scattered resistance predictions than the current codified design approaches. Lastly, the design equations adopted in EC9 for net section and block shear resistances were modified by adding the friction contribution proposed in the current paper, leading to more accurate resistance predictions. The proposed design equations in the present study offer improved design accuracy for aluminium alloy shear connections connected by the novel swage-locking pins.

Acknowledgements

The authors would like to acknowledge the financial supports provided by the National Natural Science Foundation of China (Grant No. 52108165 and No. 51878377), the Key Laboratory of

Seismic Engineering Technology in Sichuan (Grant No. ASFL-21-003) and the fund of China Huaneng Group Clean Energy Research Institute Co., Ltd. (Grant No. QNYJJ22-06).

References

[1] Mazzolani FM. Aluminium alloy structures. Second edition. London: E & FN Spon, 1995.

[2] Wang YQ, Wang ZX, Yin FX, Yang L, Shi YJ, Yin J. Experimental study and finite element analysis on the local buckling behavior of aluminium alloy beams under concentrated loads. *Thin-Walled Structures*, 2016, 105: 44-56.

[3] Miller RA. The bearing strength of steel and aluminum alloy sheet in riveted or bolted joints. *Journal of the Aeronautical Sciences*, 1937, 5(1): 22-24.

[4] Menzemer CC, Fei L, Srivatsan TS. Failure of bolted connections in an aluminum alloy. *Journal of Materials Engineering and Performance*, 1999, 8(2): 197-204.

[5] Menzemer CC, Fei L, Srivatsan TS. Mechanical response and failure of bolted connection elements in aluminum alloy 5083. *Journal of Materials Engineering and Performance*, 1999, 8(2): 211-218.

[6] Menzemer CC, Ortiz-Morgado R, Iascone R, Srivatsan TS. An investigation of the bearing strength of three aluminum alloys. *Materials Science and Engineering: A*, 2002, 327(2): 203-212.

[7] AA (Aluminium Association), Specification for Aluminium Structures: Aluminium Design Manual (ADM), Aluminium Association, Washington, DC, 2015.

[8] Wang ZX, Wang YQ, Zhang GX, Shi YJ. Tests and parametric analysis of aluminum alloy bolted joints of different material types. *Construction and Building Materials*, 2018, 185: 589-599.

[9] Kim TS, Cho YH. Investigation on ultimate strength and failure mechanism of bolted joints in two different aluminum alloys. *Materials & Design*, 2014, 58: 74-88.

[10] Cho YH, Kim TS. Estimation of ultimate strength in single shear bolted connections with aluminum alloys (6061-T6). *Thin-Walled Structures*, 2016, 101: 43-57.

[11] Hwang BK, Kim TS. An investigation on ultimate strength of high strength aluminum alloys four-bolted connections with out-of-plane deformation. *International Journal of Steel Structures*, 2019, 19(4): 1158-1170.

[12] Elghazouli AY, Málaga-Chuquitaype C, Castro JM, Orton AH. Experimental monotonic and cyclic behaviour of blind-bolted angle connections. *Engineering Structures*, 2009, 31(11): 2540-2553.

[13] Ding J, Wang YC. Experimental study of structural fire behaviour of steel beam to concrete

filled tubular column assemblies with different types of joints. *Engineering Structures*, 2007, 29(12): 3485-3502.

[14] Wang ZX, Wang YQ, Li BB, Zhang Y. Experimental and numerical study on seismic behaviour of aluminium alloy frames. *Journal of Building Engineering*, 2022, 50: 104231.

[15] Bouchaïr A, Averseng J, Abidelah A. Analysis of the behaviour of stainless steel bolted connections. *Journal of Constructional Steel Research*, 2008, 64(11): 1264-1274.

[16] Wang ZX, Wang YQ, Yun X, Gardner L, Teh LH. Experimental study of swage-locking pinned aluminium alloy shear connections. *Thin-Walled Structures*, 2021, 163: 107641.

[17] Zhang Y, Wang YQ, Li BB, Wang ZX, Liu XC, Zhang JG, Ouyang YW. Structural behaviour of the aluminium alloy Temcor joints and Box-I section hybrid gusset joints under combined bending and shear. *Engineering Structures*, 2021, 249: 113380.

[18] CEN (European Committee for Standardization). Eurocode 9: Design of aluminium structures—Part 1-1: General structural rules. 2007, *EN 1999-1-1: 2007*, Brussels.

[19] Standards Australia, Aluminium Structures Part 1: Limit State Design, AS/NZS 1664.1:1997, Sydney, Australia, 1997.

[20] MOHURD (Ministry of Housing and Urban-Rural Development of the People's Republic of China). Code for design of aluminium structures. 2007, *GB 50429-2007*, Beijing. (In Chinese)

[21] Chesson E, Munse WH. Studies of the behaviour of high strength bolts and bolted joints, 1965, University of Illinois.

[22] Reuther D, Baker I, Yetka A, Cleary DB, Riddell W. Relaxation of ASTM A325 bolted assemblies, *Journal of Structural Engineering*, 2014, 140(9), 04014060.

[23] Wang YQ, Yang L, Guan J, Zhang Y. Long-time experimental monitoring of strain relaxation of stainless steel bolts, *Journal of Shenyang Jianzhu University (Natural Science)*, 2015, 31(2), 201–208. (in Chinese)

[24] MOHURD (Ministry of Housing and Urban-Rural Development of the People's Republic of China). Technical specification for high strength bolt connections of steel structures. 2011, *JGJ 82 – 2011*, Beijing. (in Chinese)

[25] CEN (European Committee for Standardization). Execution of steel structures and aluminium structures Part 2: Technical requirements for steel structures. 2018, *EN 1090-2: 2018*, Brussels.

[26] Nah HS, Lee HJ, Kim KS. Evaluation of slip coefficient of slip critical joints with high strength bolts. *Structural Engineers and Mechanics*, 2009, 32(4): 477-488.

[27] ABAQUS. Abaqus analysis user's guide: Online documentation. Version 2017. Providence, RI: Dassault Systemes Simulia Corp, 2017.

[28] Elliott MD, Teh LH. Whitmore Tension Section and Block Shear. *Journal of Structural*

Engineering, 2019, 145(2), 04018250.

[29] Elliott MD, Teh LH, Ahmed A. Behaviour and strength of bolted connections failing in shear, *Journal of constructional steel research*, 2019, 153, 320–329.

[30] Sun EQ. Shear locking and hourglassing in MSC Nastran, ABAQUS, and ANSYS. Proc., MSC Software Corporation's 2006 Americas Virtual Product Development Conf.: Evolution to Enterprise Simulation, MSC Software, Santa Ana, CA, 2006: 1–9.

[31] Wang ZX, Wang YQ, Zhang Y, Gardner L, Ouyang YW. Experimental investigation and design of extruded aluminium alloy T-stubs connected by swage-locking pins. *Engineering Structures*, 2019, 200: 109675.

[32] Wang ZX, Wang YQ, Yun X, Zhang Y, Li ZQ, Wang ZY. Numerical modelling of extruded aluminium alloy T-stubs connected by swage-locking pins: FE validation and parametric study. *Thin-Walled Structures*, 2020, 155: 106926.

[33] Yun X, Wang ZX, Gardner L. Full-range stress–strain curves for aluminum alloys, *Journal of Structural Engineering*, 2021, 147(6), 04021060.

[34] Bruhns OT. The Prandtl‐Reuss equations revisited, *ZAMM‐Journal of Applied Mathematics and Mechanics*, 2014, 94(3): 187-202.

[35] Bao Y, Wierzbicki T. On fracture locus in the equivalent strain and stress triaxiality space, *International Journal of Mechanical Sciences*, 2004, 46(1): 81-98.

[36] Ghahremaninezhad A, Ravi-Chandar K. Ductile failure behavior of polycrystalline Al 6061-T6 under shear dominant loading, *International Journal of Fracture*, 2013, 180(1): 23-39.

[37] Khan FI. Failure modeling of the tubular expansion process [Master dissertation]. United Arab Emirates, Abu Dhabi: The Petroleum Institute, 2012.

[38] Chen X, Peng Y, Peng S, Yao S, Chen C, Xu P. Flow and fracture behavior of aluminum alloy 6082-T6 at different tensile strain rates and triaxialities. *PloS one*. 2017, 12(7): e0181983.

[39] Zhang W, Xiao XK, Wei G. Constitutive relation and fracture model of 7A04 aluminum alloy, *Explosion and Shock Waves*, 2011,31(1),81-87. (in Chinese)

[40] Ramberg W, Osgood WR. Description of Stress-Strain Curves by Three Parameters. Technical Note No. 902. Washington, D.C., USA: National Advisory Committee for Aeronautics; 1943.

[41] Deng H, Chen WG, Bai GB, Dong SL. Experimental study on shearing behaviour of lockbolted lap connection for aluminium alloy plates. *Journal of Building Structures*, 2016, 37 (1): 143-149. (in Chinese)

[42] Teh LH, Uz ME. Combined bearing and shear-out capacity of structural steel bolted connections. *Journal of Structural Engineering*, 2016, 142(11): 04016098.

[43] Zhang GX. Analysis and design methods of bolted connection in aluminum alloy subjected to shear and tensile force [Master dissertation]. Beijing: Tsinghua University, 2006. (in Chinese)

[44] Teh LH, Uz ME. Ultimate shear-out capacities of structural-steel bolted connections. *Journal of Structural Engineering*, 2015, 141(6): 04014152.

[45] Cai Q, Driver RG. Prediction of bolted connection capacity for block shear failures along atypical paths. *Engineering Journal-Chicago*, 2010, 47(4):213-221.

[46] ANSI/AISC 360-16. Specification for structural steel buildings. Chicago: American Institute of Steel Construction. 2016.

[47] Aalberg A, Larsen PK. Bearing strength of bolted connections in high strength steel. *Proc. 9th Nordic Steel Construction Conf.*, Helsinki, Finland, 2001: 859–866.

[48] Rex CO, Easterling WS. Behavior and modelling of a bolt bearing on a single plate. *Journal of Structural Engineering*, 2003, 129(6): 792–800.

[49] Kim HJ, Yura JA. (1999). The effect of ultimate-to-yield ratio on the bearing strength of bolted connections. *Journal of Constructional Steel Research*, 1999, 49(3): 255–269.

[50] Teh LH, Uz ME. Effect of loading direction on the bearing capacity of cold-reduced steel sheets. *Journal of Structural Engineering*, 2014, 140(12), 06014005.

[51] Yang L, Wang YQ, Guan J, Zhang Y, Shi YJ. Bearing strength of stainless steel bolted connections. *Advances in Structural Engineering*, 2015, 18(7): 1051-1062.